# Report: Medida del ángulo de contacto

J. Torrent Burgués, Depto Ingeniería Química, FOOT-UPC, Terrassa

**Resumen**

El ángulo de contacto es un parámetro que se usa en materiales para caracterizar las propiedades de humectabilidad de éstos. La medida del ángulo de contacto es por ello importante, en especial en biomateriales. También sirve para observar el efecto de modificaciones en las superficies, bien sea por tratamientos o por deposición de películas de otros materiales o capas moleculares. En este artículo se expone la técnica de medida utilizando un montaje realizado por el autor, y se ha aplicado a varios sustratos, entre los que se han incluido algunos usados como materiales ópticos. También se ha realizado una búsqueda bibliográfica sobre el ángulo de contacto y su medida y significación.

# 1. Ángulo de contacto sobre varios materiales inorgánicos y orgánicos.

## Introducción

El ángulo de contacto (Figura 1) es un parámetro fundamental para caracterizar las propiedades de hidrofilicidad, humectación y biocompatibilidad en los materiales. La expresión que liga el ángulo de contacto de un líquido sobre un sólido con las tensiones superficiales del sólido ($\gamma_S$), del líquido ($\gamma_L$) e interfacial sólido/líquido ($\gamma_{S/L}$) (Figura 1) es [1-3]:

$$\cos\theta = \frac{\gamma_S - \gamma_{L/S}}{\gamma_L} \qquad (1)$$

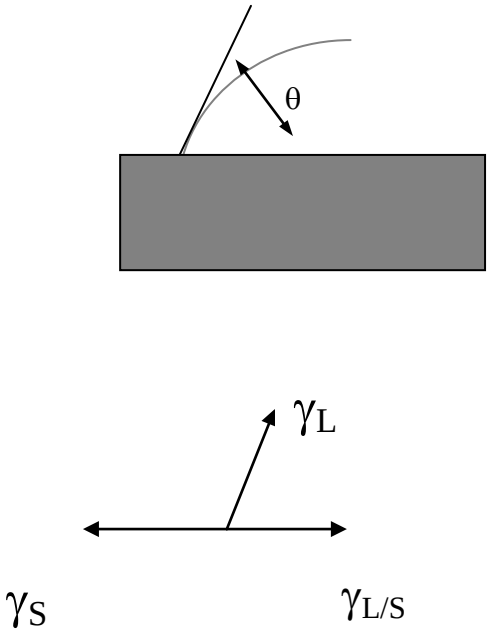


**Figura 1**. Esquema del ángulo de contacto, y de las tensiones que actúan en la línea de contacto entre sólido, líquido y aire.

De acuerdo con dicha ecuación, una disminución del ángulo de contacto (cosθ aumenta), y por tanto un aumento en la humectación, puede conseguirse con un

aumento de la tensión superficial del sólido ($\gamma_S$), con una disminución de la tensión superficial del líquido ($\gamma_L$), con una disminución de la tensión interfacial sólido/líquido ($\gamma_{S/L}$), o con una adecuada combinación entre estas. Como los materiales ópticos inorgánicos tienen una tensión superficial $\gamma_S$ mayor que los materiales ópticos orgánicos, los segundos presentan ángulos de contacto mayores. Por tanto, su uso en lentes de contacto suele conllevar algún problema de humectabilidad y requiere de procesos para su mejora. Un aumento de la humectabilidad puede conseguirse haciendo que la superficie sea más hidrofílica, lo cual a la vez que comporta un aumento de $\gamma_S$ también suele comportar una disminución de $\gamma_{S/L}$. Por otro lado, para un aumento de la humectabilidad también puede buscarse una disminución de $\gamma_L$, lo cual se consigue con la introducción de humectantes en las soluciones de acondicionamiento o con lágrimas artificiales; estas sustancias también suelen producir una disminución de $\gamma_{S/L}$, y por tanto contribuyendo por esta segunda vía a un aumento de la humectación.

Para la medida del ángulo de contacto existen básicamente dos grupos de métodos. Uno consiste en la medida del $\theta$ por la técnica de la gota en aire (o gota sésil), mientras que el otro realiza la medida del $\theta$ por la técnica de la burbuja cautiva. El primero es más general y fácil de usar, siendo más apropiado para materiales con bajo o nulo contenido en agua, mientras que el segundo requiere de un montaje más elaborado y se aplica para materiales con un importante contenido en agua, ya que mantiene las condiciones de hidratación. Por otro lado, la técnica de la gota en aire es más apropiada para la medida del ángulo de contacto de avance, o sobre superficie seca, mientras que la técnica de la burbuja cautiva es más apropiada para la medida del ángulo de retroceso, o sobre una superficie humectada. Sin embargo, ambas técnicas pueden servir para la medida de ambos valores del $\theta$ con las oportunas consideraciones.

En este trabajo se ha usado un equipo para la medida del ángulo de contacto, y se ha aplicado a una serie de materiales, algunos de ellos usados como materiales ópticos.

**Experimental**

Para la medida de ángulos de contacto se ha utilizado la técnica de la gota en aire. Para ello se ha montado un microscopio en banco horizontal y una fuente de iluminación

adecuada, con una cámara CCD acoplada al ocular y conectada a un ordenador. Las imágenes captadas han sido usadas posteriormente para determinar el valor del ángulo de contacto (Figura 2a). Las gotas, de un volumen definido, generalmente pequeño y de alrededor de 2 microlitros, se depositaron sobre el substrato con ayuda de una micropipeta. El agua utilizada es agua ultrapura. Los substratos se limpiaron previamente con detergente y se enjuagaron con mucha agua, después se enjuagaron con alcohol y de nuevo con agua; a continuación se eliminó el exceso de agua con papel absorbente, se dejaron secar al aire y finalmente se hizo pasar una corriente de aire por encima de la superficie de los substratos.

En los experimentos se usaron diferentes substratos y diferentes líquidos, detallados en el apartado de resultados y discusión y en las tablas. Para el valor de θ se realizaron medidas tanto en el lado derecho como en el izquierdo de la gota (Figura 2b), y además repitiendo la gota, y tomando al final el valor promedio. La temperatura de trabajo fue la temperatura ambiente de 22-23ºC.

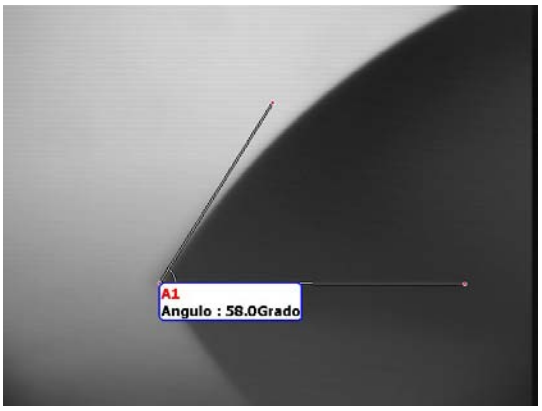


**Figura 2.** a) Método de medida del ángulo de contacto, imagen ampliada.

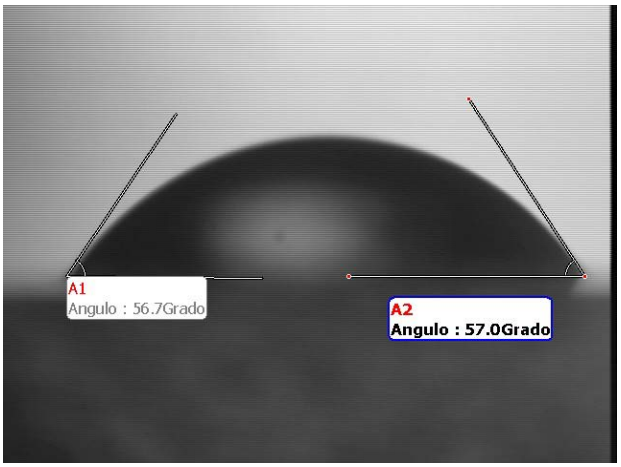


**Figura 2.** b) Método de medida del ángulo de contacto, ambos lados.

## Resultados y discusión

*Influencia del substrato*

Se han realizado medidas de ángulo de contacto sobre varios substratos inorgánicos, tales como vidrio, mica o nitruro de silicio. Los valores medidos se recogen en la tabla I.A, con la indicación de la figura correspondiente. Los resultados muestran que estas superficies son bastante hidrofílicas, aunque en mayor o menor grado según el material. De entre ellos, destaca la mayor hidrofilicidad de la mica, un mineral fácilmente exfoliable formado por silicato de potasio y aluminio ($KAl_3H_2(SiO_4)_3$), con el ángulo de contacto menor, después viene el vidrio (formado por óxido de silicio ($SiO_2$), óxido de sodio ($Na_2O$) y óxido de calcio (CaO)) y después el nitruro de silicio ($Si_3N_4$), por orden creciente de ángulo de contacto y por tanto en orden decreciente de humectabilidad. El valor obtenido para el nitruro de silicio concuerda con los valores reportados en la bibliografía, que oscilan entre 48º y 55º. Ahora bien, cuando el nitruro de silicio se somete a un lavado con ácido fluorhídrico (HF) y especialmente con solución piraña (mezcla de ácido sulfúrico y agua oxigenada), se obtienen ángulos de contacto más bajos, del orden de los del vidrio o incluso inferiores, lo cual indica que estos reactivos atacan la superficie del nitruro de silicio y la vuelven más hidrofílica.

Tabla I. A) ángulos de contacto de agua sobre materiales inorgánicos
B) ángulos de contacto de agua sobre materiales orgánicos

| **A** | θ avance | **B** | θ avance | θ lente (retroceso) |
|---|---|---|---|---|
| Mica | 18º (Fig 3a) | PMMA 1 | 65º (Fig 4) | |
| Vidrio * | 42º (Fig 3b) | PMMA 2 | 73º | |
| Nitruro de silicio | 51º (Fig 3c) | Boston Equalens II | 103º (Fig 5a) | 30º |
| Nitruro de silicio 2 | 45º | Boston Lens IV | 71º (Fig 5b) | 17º |
| Nitruro de silicio 3 | 32º | Boston RXD | 112º (Fig 5c) | 39º |
| | | Boston 7 | 113º (Fig 5d) | 54º |

Vidrio *: corresponde a un vidrio de portaobjetos; Nitruro de silicio 2: atacado con HF; Nitruro de silicio 3: atacado con solución piraña.
Equalens II: oprifocon A; Lens IV: itafocon B; RXD: bisflourofocon A; Boston 7: satafocon A.

Figuras 3 a, b, c

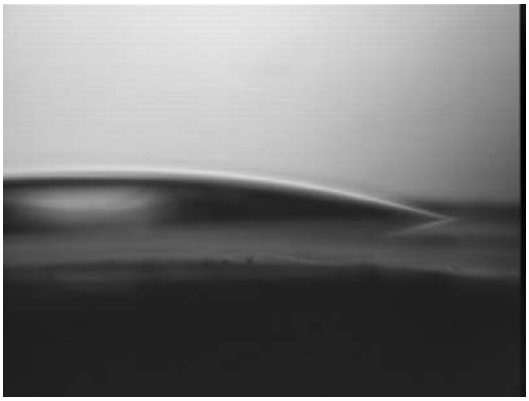
Figura 3.a) Gota de agua sobre mica.

---

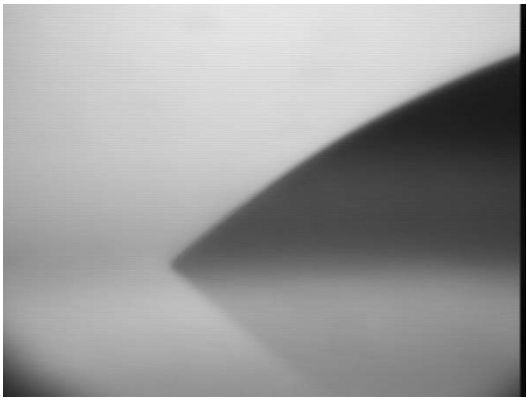
Figura 3.b) Gota de agua sobre vidrio porta.

---

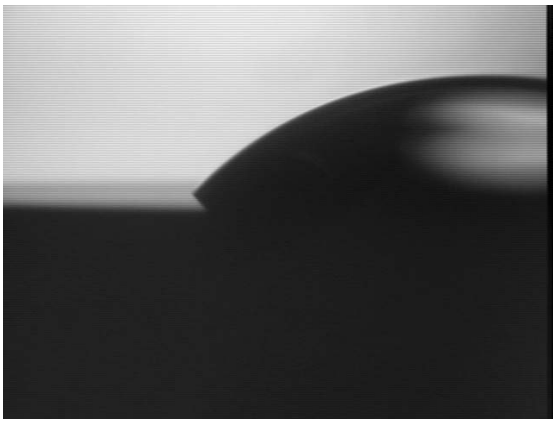
Figura 3.c) Gota de agua sobre nitruro de silicio.

También se han realizado medidas de ángulo de contacto sobre varios substratos orgánicos, tales como PMMA y otros utilizados como materiales ópticos, comercializados como Boston Equalens II, Boston Lens IV, Boston 7 y Boston RXD, todos ellos en forma de taco cilíndrico (Tabla I.B). Los materiales orgánicos estudiados muestran ángulos de contacto más grandes o mucho más grandes que los materiales inorgánicos. Y entre los materiales orgánicos se observa que el PMMA y el Boston Lens IV presentan un ángulo de contacto menor, y por tanto mejor humectación, que los otros, los cuales presentan ya un ángulo de contacto superior a 90º. Hay que mencionar que estos valores son diferentes a los que aparecen en los catálogos comerciales para las lentes de contacto de estos materiales; ello es debido a que aquí se han medido sobre un taco macizo del material, sin hidratar, mientras que los reportados en los catálogos son para el material preparado para su uso, y generalmente medido con la técnica de la burbuja cautiva, la cuál proporciona ángulos de retroceso, es decir, sobre superficie humectada, y por tanto menores (ver Tabla I). Sin embargo, se observa una correlación entre ambas series de valores. En lo que respecta al PMMA, el valor medido para la muestra PMMA2 concuerda con el reportado en la bibliografía. La diferencia entre los dos valores medidos es debido a que son muestras de diferente procedencia, y por tanto pueden ser diferentes. A la vista de los valores medidos, en las mismas condiciones experimentales, y del reportado en la bibliografía, podemos concluir que el PMMA1 debe estar modificado por algún tipo de aditivo que lo hace ligeramente más hidrofílico.

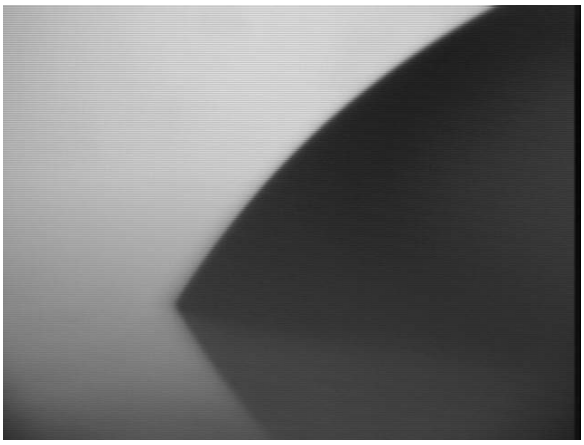

Figura 4. Gota de agua sobre PMMA.

Figuras 5 a, b, c, d

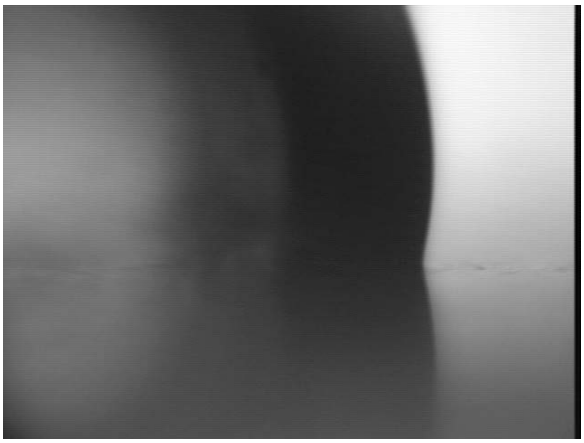

Figura 5.a) Gota de agua sobre Boston equalens II.

---

Figura 5.b) Gota de agua sobre Boston Lens IV.

---

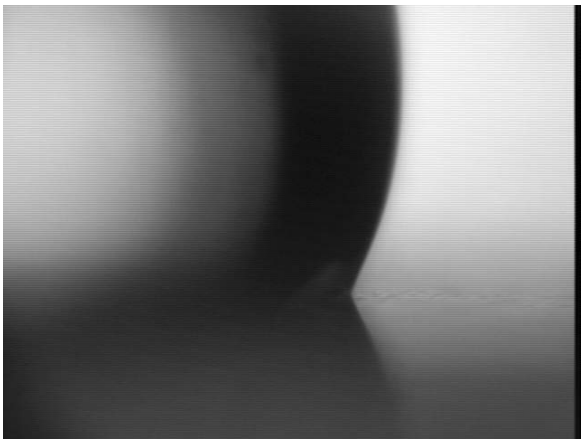

Figura 5.c) Gota de agua sobre boston RXD.

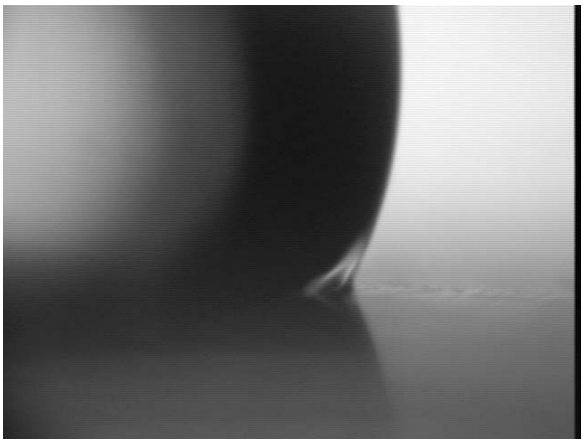

Figura 5.d) Gota de agua sobre Boston 7.

*Influencia del líquido*

Otro factor que determina el ángulo de contacto es el líquido de la gota. La composición de éste afecta a las tensiones superficiales y por tanto al ángulo de contacto, aunque se mantenga el substrato, tal como se refleja en la ecuación (1). En la tabla II se indican los ángulos de contacto obtenidos con algunos de los substratos anteriormente estudiados, pero utilizando ahora una solución salina concentrada y una solución de cloruro de benzalconio (BAK), un tensioactivo o surfactante con propiedades conservantes y que se utiliza en algunas soluciones de lentes de contacto.

Tabla II. Valores de ángulo de contacto de avance para varios substratos y varios líquidos

| | θ solución 12% NaCl | θ solución 0,1% BAK |
|---|---|---|
| PMMA1 | 67 | 22 |
| Vidrio porta | 45 | 14 |

Se observa que la solución de cloruro sódico (NaCl), aunque muy concentrada, afecta poco al valor del ángulo de contacto, pero haciendo que éste aumente ligeramente. De acuerdo con la ecuación (1), esto es debido al ligero aumento que las sales tipo NaCl provocan en la tensión superficial del agua. Por contra, la solución de BAK, aunque con una concentración mucho más baja que la anterior de cloruro sódico, presenta un marcado descenso del ángulo de contacto. Esto es debido al efecto tensioactivo o surfactante de esta sustancia, que provoca un notable descenso en la tensión superficial del agua. En la bibliografía encontramos que una solución de BAK al 0.004%, la típica en soluciones de lentes de contacto, presenta un ángulo de contacto de 40º sobre PMMA. Como para estas sustancias el ángulo de contacto disminuye al aumentar la concentración, el resultado obtenido por nosotros sigue perfectamente esta tendencia.

*El θ como técnica de análisis superficial*

En un apartado anterior se ha comentado como el tratamiento previo de una superficie influye en el valor del ángulo de contacto que ésta presentará, puesto que el tratamiento puede modificar el estado y características de la superficie. La medida del ángulo de contacto puede aplicarse como una técnica para analizar el estado o características de una superficie que no conocemos bien. En la figura 6 se presenta el ángulo de contacto que una gota de agua forma sobre un vidrio mineral de densidad 2,5 g/cm$^3$, la de un vidrio mineral típico. El valor medido de θ=55º es superior al de un vidrio mineral típico, lo cual indica que existe un recubrimiento sobre dicho vidrio. Esta hipótesis viene reforzada por la observación óptica, con unas propiedades de transmisión y reflexión diferentes a las del vidrio mineral típico. Las medidas del ángulo de contacto realizadas con solución salina y de BAK sobre dicho vidrio, también confirman unas características superficiales diferentes, a la vez que añaden más información. El ángulo de contacto medido con la solución salina es de 40º, un valor bastante inferior al anterior y que muestra una tendencia opuesta a la observada y comentada en el apartado

previo, en que la solución salina hacia aumentar ligeramente el ángulo de contacto. Por otro lado, el ángulo de contacto con la solución de BAK es similar o incluso ligeramente superior a la del vidrio mineral. Estos hechos nos vienen a indicar que la notable disminución del θ con la solución salina, que no puede atribuirse a la tensión superficial del líquido, $\gamma_L$, según la ecuación (1), ha de ser debida a una notable disminución de la tensión interfacial líquido/sólido, $\gamma_{L/S}$. Por tanto, el tipo de recubrimiento presente muestra mayor afinidad por la solución salina, indicando que la superficie del vidrio recubierto interacciona bien con los iones de la solución salina, y por tanto debe tratarse de un recubrimiento inorgánico y no orgánico, como cabria esperar al principio al observarse un ángulo de contacto mayor con el agua. También el ligero aumento en el ángulo de contacto con la solución de BAK apunta a que no se trata de un recubrimiento orgánico, sino de tipo inorgánico.

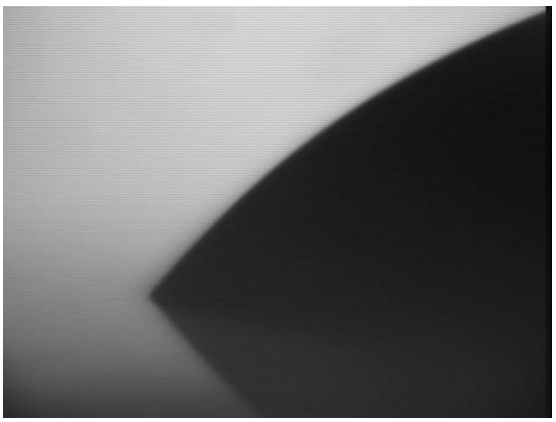

Figura 6. Gota de agua sobre vidrio recubierto desconocido.

*Histéresis del ángulo de contacto*

Un fenómeno interesante e importante relacionado con el ángulo de contacto es que su valor depende del estado de la superficie del material. En concreto, en ciertos materiales se obtiene un valor diferente del ángulo si la gota se forma sobre una superficie seca o sobre una superficie previamente humectada. En la técnica de la gota en aire, cuando se forma la gota ésta encuentra una superficie seca, y el valor del θ medido corresponde al ángulo de avance $\theta_a$. En cambio, si la gota una vez formada va retrocediendo se

encuentra con una superficie ya humectada, que ha estado en contacto con el líquido, y el valor del θ medido corresponde al ángulo de retroceso $\theta_r$, el cual es menor. A este fenómeno se le conoce como histéresis del ángulo de contacto, siendo $\theta_r<\theta_a$.

El fenómeno de histéresis ha sido observado en varios de los substratos citados en los apartados anteriores. Sin embargo, el proceso utilizado no nos ha permitido obtener el valor final o de equilibrio para $\theta_r$, sino solo la variación del ángulo durante un cierto intervalo de tiempo, mientras la gota de agua iba retrocediendo. En la Figura 7 se muestran dichas variaciones tanto para los materiales orgánicos como para los inorgánicos. Tal como hemos indicado, los valores medidos no corresponden al estado estacionario o de equilibrio; por ejemplo, para el PMMA el valor medido al cabo de 1 min es de 59º, mientras que el valor de $\theta_r$ reportado en la bibliografía es de 40º. Es decir, se requiere un cierto tiempo para que la superficie humectada llegue al estado estacionario o de equilibrio. En la Figura 7 también se ha representado la variación del ángulo del vidrio mineral con recubrimiento analizado anteriormente; éste presenta una notable histéresis del θ, llegando a rebajar su valor desde 55º hasta 35º al cabo de 1,5 min. De todos los materiales analizados, éste es el que presenta una mayor histéresis de θ, lo cuál nos aporta más información sobre las características del recubrimiento que lleva el vidrio base.

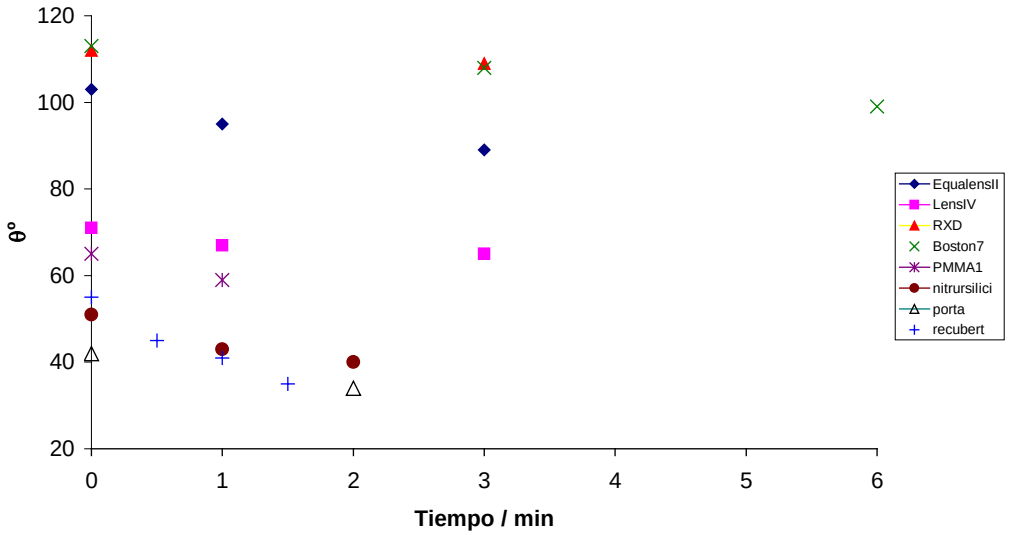


Figura 7. Variación del θ de la gota de agua durante el retroceso, sobre diferentes materiales. 1 (◆): Boston Equalens II, 2 (■): Boston Lens IV, 3 (▲): Boston RXD, 4 (X): Boston 7, 5 (✳): PMMA1; a (●): Nitruro de silicio, b (△): Vidrio porta, c (+): Vidrio recubierto.

## Bibliografía

[1] J. Torrent. Química de superficies. Tratamientos superficiales. Publicaciones de la EUOOT, Terrassa, 1992.

[2] a) A.W. Adamson. Physical chemistry of surfaces, John Wiley & Sons, 1982. b) D.J. Shaw. Introducción a la química de superficies y coloides. Alhambra, 1977.

[3] J. Torrent. Ver y Oír septiembre 2003, pg 478.

## Tablas

Tabla I. A) ángulos de contacto de agua sobre materiales inorgánicos
B) ángulos de contacto de agua sobre materiales orgánicos

| **A** | θ avance | **B** | θ avance | θ lente (retroceso) |
|---|---|---|---|---|
| Mica | 18º (Fig 3a) | PMMA 1 | 65º (Fig 4) | |
| Vidrio * | 42º (Fig 3b) | PMMA 2 | 73º | |
| Nitruro de silicio | 51º (Fig 3c) | Boston Equalens II | 103º (Fig 5a) | 30º |
| Nitruro de silicio 2 | 45º | Boston Lens IV | 71º (Fig 5b) | 17º |
| Nitruro de silicio 3 | 32º | Boston RXD | 112º (Fig 5c) | 39º |
| | | Boston 7 | 113º (Fig 5d) | 54º |

Vidrio *: corresponde a un vidrio de portaobjetos; Nitruro de silicio 2: atacado con HF; Nitruro de silicio 3: atacado con solución piraña.
Equalens II: oprifocon A; Lens IV: itafocon B; RXD: bisflourofocon A; Boston 7: satafocon A.

Tabla II. Valores de ángulo de contacto de avance para varios substratos y varios líquidos

| | θ solución 12% NaCl | θ solución 0,1% BAK |
|---|---|---|
| PMMA1 | 67 | 22 |
| Vidrio porta | 45 | 14 |

# 2. Propiedades de disoluciones de BAK

**Resumen**

Propiedades fisicoquímicas tales como la tensión superficial y el ángulo de contacto de disoluciones de cloruro de benzalconio (BAK), usado en soluciones para lentes de contacto, han sido medidas, pudiéndose establecer una relación entre ambas. Tanto la tensión superficial como el ángulo de contacto muestran una fuerte dependencia con la concentración para disoluciones diluidas, pero superada una cierta concentración, conocida como concentración micelar crítica (cmc), esta dependencia es muy débil o nula. El tratamiento de los datos permite determinar dicha cmc.

**Introducción**

Las soluciones para lentes de contacto desempeñan un papel importante dentro de la contactología. Existen diferentes tipos de soluciones, según el tipo de lente de contacto a la que van destinadas y según la función específica requerida. Por tanto, la composición de la solución depende en gran medida de estos factores. En una solución de lentes de contacto, el agua es el componente mayoritario, o disolvente, pero después existen los componentes minoritarios, o solutos, cada uno con una función determinada.

Ciertas sustancias, conocidas como surfactantes o tensioactivos, ejercen una gran influencia sobre la tensión superficial del agua, y sus disoluciones presentan una disminución notable de la tensión superficial, incluso a muy bajas concentraciones. Si $\gamma_o$ es la tensión superficial del agua pura y $\gamma$ la de la disolución, la diferencia entre ambas recibe el nombre de presión superficial.

$$\pi=\gamma_o-\gamma \qquad (1)$$

Los tensioactivos presentan una estructura química con una parte apolar o hidrofóbica, generalmente una cadena hidrocarbonada, y una parte polar o hidrofílica, generalmente

un grupo funcional orgánico polar o capaz de ionizarse en disolución. Estos compuestos se concentran en la superficie del agua con el aire y provocan la disminución de γ. Entre las aplicaciones prácticas destacan su acción de limpieza o detergente, y algunos de ellos, como las sales de alquilamonio, también se usan como conservantes en soluciones de lentes de contacto. El cloruro de benzalconio, o BAK, es una sal de alquilamonio, en concreto de alquilbencildimetilamonio, con la fórmula molecular indicada en el esquema 1. El BAK aparece en la formulación de ciertas soluciones de lentes de contacto, junto a otros componentes, y su concentración suele ser muy baja, alrededor del 0,004%; a pesar de ello, su efecto en las propiedades fisicoquímicas es ya notable y ejerce una acción conservante efectiva, pero sin que pueda provocar efectos perjudiciales en la lente de contacto o en su aplicación en el ojo.

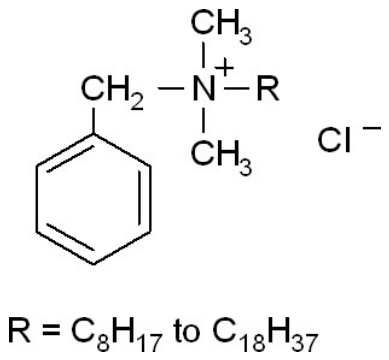


Esquema 1. Fórmula del cloruro de benzalconio.

Los tensioactivos también tienen influencia en el ángulo de contacto, θ, es decir en la forma que adopta una gota de disolución cuando se coloca sobre una superficie sólida (Figura 1). El ángulo de contacto depende, según la ecuación 2, de la tensión superficial de la disolución $\gamma_L$ y de la tensión interfacial entre ésta y el sólido $\gamma_{L/S}$, y en ambos casos el tensioactivo puede ejercer una notable influencia [1].

$$\cos\theta = \frac{\gamma_S - \gamma_{L/S}}{\gamma_L} \qquad (2)$$

En este trabajo se realiza un estudio de disoluciones de BAK preparadas en el laboratorio, donde éste es el único soluto presente, con lo que se puede analizar sin

ambigüedad el efecto de este componente. Se han medido los valores de tensión superficial y de ángulo de contacto para disoluciones acuosas de BAK, en función de la concentración, y se han correlacionado los resultados obtenidos para ambas magnitudes.

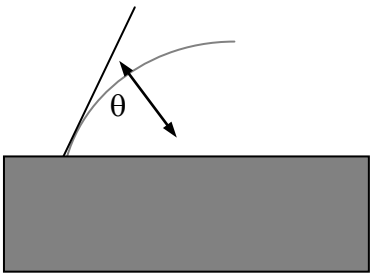


A

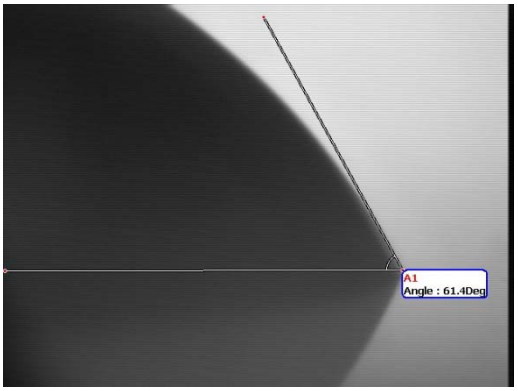


B

Figura 1. A) Esquema del ángulo de contacto, B) Medida del ángulo de contacto

**Experimental**

Las medidas de presión superficial se realizaron usando como tensiómetro una balanza de Wilhelmy (Figura 2) incorporada a un equipo NIMA. La temperatura de trabajo ha sido de 27ºC. En primer lugar se introduce la placa de Wilhelmy en agua y se toma como cero; a continuación se reemplaza el agua por una disolución de BAK, sin variar ningún parámetro geométrico del sistema, y se toma lectura del valor de presión superficial $\pi$ que mide la balanza. En este trabajo se ha tomado como criterio coger los valores iniciales de $\pi$, aunque éstos experimentan una cierta variación con el tiempo. Un estudio detallado de esta variación se deja para trabajos posteriores. El valor de $\gamma$ se

obtiene con la ecuación 1. A partir de los valores tabulados de la tensión superficial del agua y su dependencia con la temperatura se puede obtener γo, que en nuestro caso, a 27ºC, resulta ser:

$\gamma o(27ºC)=\gamma o(20ºC)+d\gamma/dT*(T-20)=72,88-0,138*(27-20)=71,91\approx71,9$ mN/m.

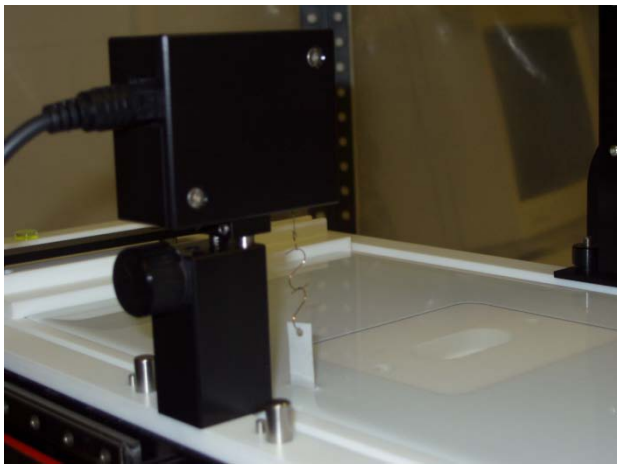

Figura 2. Balanza de Wilhelmy

Las medidas de ángulo de contacto se realizaron con un microscopio invertido acoplado a una cámara CCD para registrar las imágenes, las cuales fueron tratadas posteriormente para obtener los valores de θ. Se buscaron los objetivos y oculares y la iluminación adecuados para obtener las imágenes ópticas. La técnica utilizada para la medida de θ es la de la gota en aire [2]. La medida del ángulo de contacto se realizó justo después de formar la gota. La gota se obtuvo usando una micropipeta y depositando un volumen fijo de líquido sobre una superficie plana y limpia de PMMA.

Las disoluciones de BAK se han preparado a partir del reactivo químicamente puro, calidad QP de Panreac, y de agua ultrapura. El rango de concentraciones varía desde 0 a 0,1% en peso.

**Resultados y discusión**

Los valores de $\gamma$ y de $\theta$, medido sobre PMMA, obtenidos para las diferentes concentraciones de BAK se muestran en la Tabla 1. En la Figura 3 se recogen las imágenes de las gotas formadas. En la Figura 4 puede observarse cómo evolucionan estas magnitudes con la concentración; en ella puede observarse que a bajas concentraciones de BAK hay una fuerte influencia de la concentración sobre la tensión superficial y sobre el ángulo de contacto, y que a medida que la concentración aumenta esta dependencia es menor e incluso se hace muy pequeña o prácticamente nula. Este comportamiento es típico de tensioactivos, y ello se debe a que las moléculas de tensioactivo, las cuales presentan una cadena hidrofóbica importante, tienden a agregarse formando micelas (esquema 2) para minimizar la mala interacción de las cadenas hidrofóbicas con el agua y en cambio favorecer la buena interacción que existe entre ellas. El fenómeno de la micelación se produce de forma significativa a partir de una cierta concentración, que se conoce como concentración micelar crítica, cmc. Cuando se forman dichas micelas, la concentración de tensioactivo libre es prácticamente constante y las propiedades superficiales de la disolución prácticamente no cambian.

Tabla 1. Valores de presión superficial, tensión superficial y ángulo de contacto, medido sobre PMMA, a 27ºC para diferentes concentraciones de BAK.

| $C_{BAK}$ (% peso) | $\pi$ (mN/m) | $\gamma$ (mN/m) | $\theta$ (grados) |
|---|---|---|---|
| 0 | 0 | 71,9 | 66 |
| 0,002 | 6,5 | 65,4 | 53 |
| 0,004 | 13,6 | 58,3 | 47 |
| 0,01 | 24,7 | 47,2 | 38 |
| 0,02 | 31,5 | 40,4 | 37 |
| 0,05 | 38,0 | 33,9 | 36 |
| 0,1 | 38,7 | 33,2 | |

Para determinar dicha cmc se suele representar la tensión superficial frente al logaritmo de la concentración. En esta representación (Figura 5) se suele observar dos tramos bastante lineales, uno a más bajas concentraciones, por debajo de la cmc, y otro a más

altas concentraciones, por encima de la cmc. La intersección de las rectas de ambos tramos da un valor para la cmc. A partir de la gráfica de la Figura 5 se obtiene que para el BAK, a 27ºC, la cmc es de 0,035% en peso. Este valor no puede pasarse correctamente a concentración molar ya que en la fórmula del BAK (esquema 1) la cadena R no está bien definida. Ahora bien, tomando un valor promedio para la masa molecular del BAK, la cmc en concentración molar es aproximadamente $1{,}0\ 10^{-3}$ M. Este valor es del orden del obtenido para otros tensioactivos similares al BAK [3, 4]. Por otro lado, podemos constatar que la concentración normalmente usada en las disoluciones comerciales es bastante inferior a la cmc, por lo que podemos asegurar que en éstas no se produce micelación.

En la figura 4 puede también observarse que la variación que experimenta la tensión superficial con la concentración es bastante similar a la que experimenta el ángulo de contacto, lo cual se debe a la estrecha relación entre ambas magnitudes (ver ecuación 2). Además, esto nos indica que en la ecuación 2 el parámetro de tensión que más influye en el ángulo de contacto, para nuestro caso, es la tensión superficial de las disoluciones de BAK ($\gamma_L$), especialmente para las concentraciones más bajas.

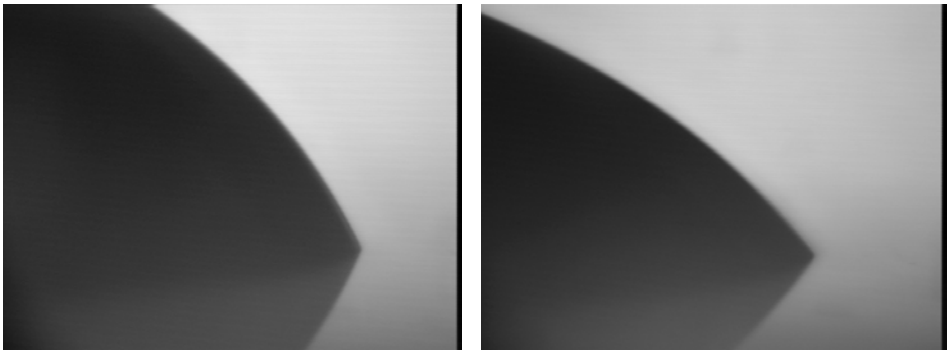

a b

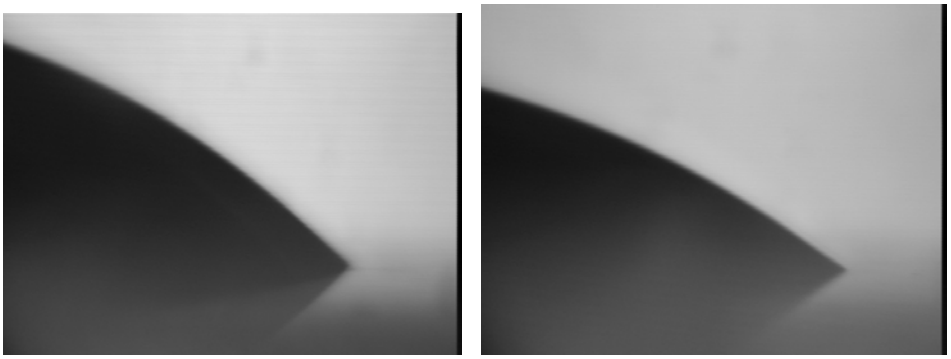

c d

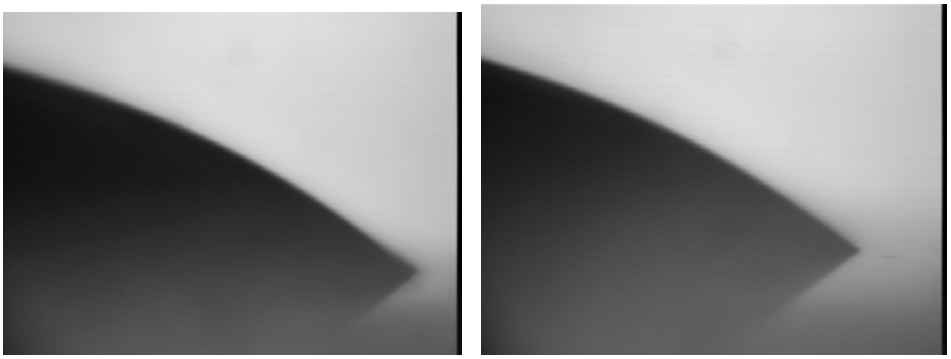

e f

Figura 3. Imágenes de las gotas formadas por disoluciones acuosas de BAK a las concentraciones de: a) 0%, b) 0,002%, c) 0,004%, d) 0,01%, e) 0,02%, f) 0,05%.

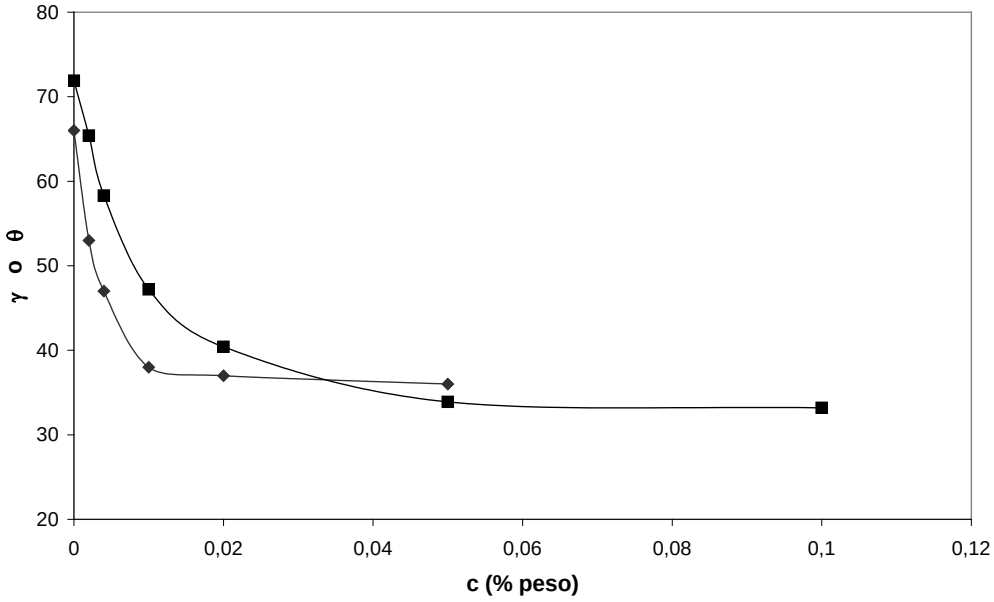


Figura 4. Variación de la tensión superficial, γ en mN/m (■), y del ángulo de contacto, θ en grados (◆), con la concentración de disoluciones acuosas de BAK.

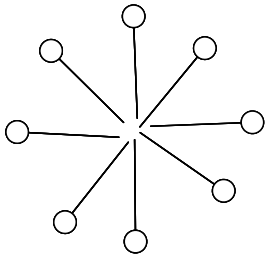

Esquema 2. Micela

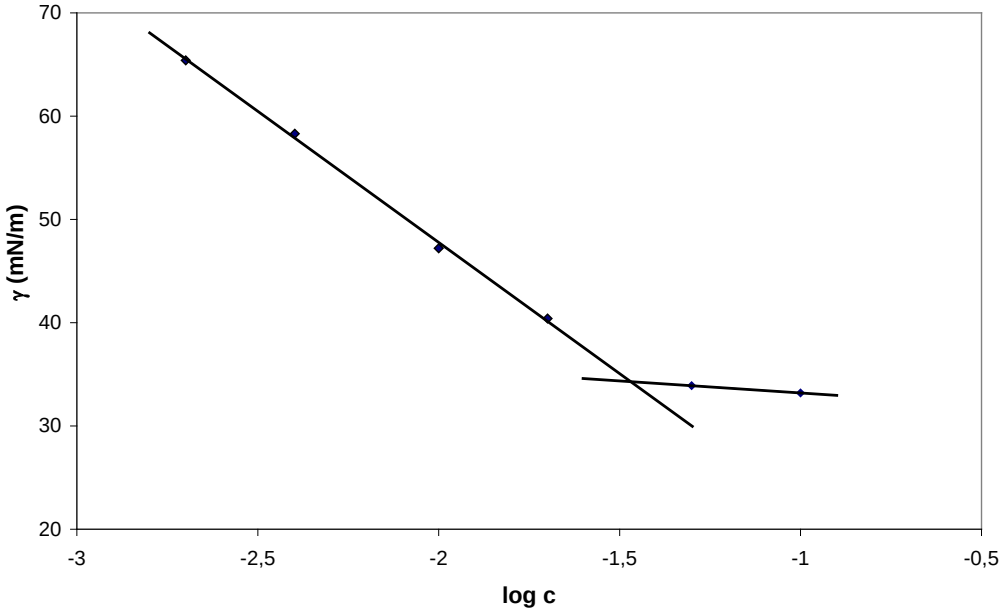


Figura 5. Tensión superficial frente al logaritmo decimal de la concentración.

**Bibliografía**

[1] J. Torrent, Películas y ultrapelículas en sistemas ópticos, Ver y Oír, septiembre 2003, pg 478

[2] J. Torrent, J. Antó, Medida del ángulo de contacto en materiales ópticos. Ver y Oír, enero-febrero 2007, pg 6

[3] M.V. Dmitrovskaya, N.N. Kochurova, G. Petzold, Colloid J. 66 (2004) 531

[4] R.M. Pashley, M.E. Karaman, Applied Colloid and Surface Chemistry, John Wiley & Sons, 2004.

## 3. Superficies modificadas con capas delgadas o moleculares.

**Abstract**

Thin films of a tetrasubstituted zinc phthalocyanine (zinc 2,9,16,23-tetra-tert-butyl-29H,31H-phthalocyanine) have been obtained using several techniques, such as adsorption, drop casting and Langmuir-Blodgett. Contact angles were measured to observe the modifications introduced by the layer formed.

**Experimental**

Thin films of a t-BuPcZn, zinc 2,9,16,23-tetra-tert-butyl-29H,31H-phthalocyanine (Figure 1), M=802.34, were obtained following different procedures. The compound t-BuPcZn was supplied by Sigma-Aldrich. Water was of ultrapure quality (Millipore-MilliQ) and chloroform was of PA grade. Solutions of t-BuPcZn in chloroform were prepared at several concentrations. Mica and HOPG (supplied by NT-MDT) sheets were cleaved before use.

Some films were obtained spreading a drop of a 0.022 mg/mL ($2.7\ 10^{-5}$ M) solution of t-BuPcZn in chloroform on mica or HOPG sheets (solvent-cast films). Other films were obtained by using the Langmuir-Blodgett film technique with a Nima 1312D1D2 equipment. The films at the air-water interphase were obtained by spreading a 0.9 mg/mL ($1.1\ 10^{-3}$ M) or a 0.26 mg/mL ($3.2\ 10^{-4}$ M) solution in chloroform, and then compressed until a certain surface pressure and finally extracted using mica or HOPG sheets.

Contact angles were also measured on mica, HOPG and thin films of t-BuPcZn, placing a water drop of 1 μL on the corresponding substrate.

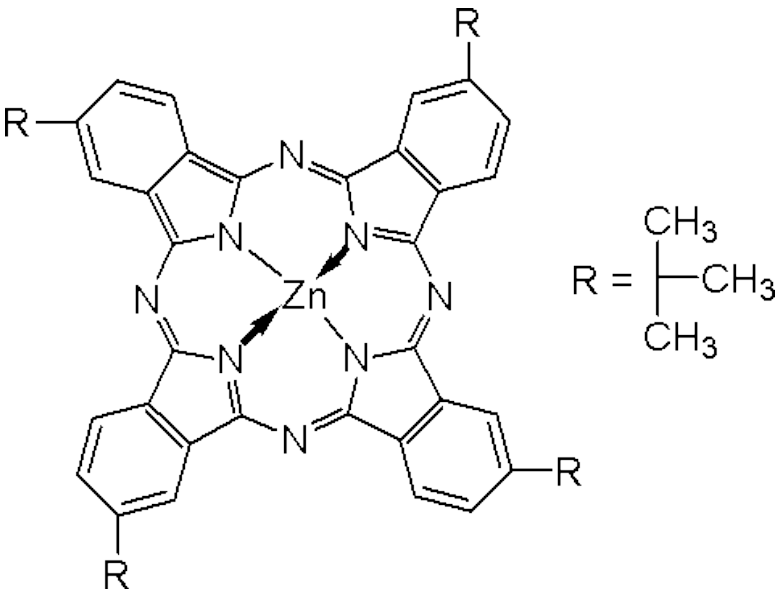


Figure 1. Structural formula of the t-BuPcZn

**Contact angle**

Contact angle measurements were done on mica and on graphite, and later on these substrates coated with a film of the t-buznpc (Figure 14). Contact angles were measured on films transferred by the LB technique. It is seen than the film increases the contact angle respect to mica, becoming more hidrophobic, but decreases the contact angle respect to graphite, becoming more hidrophilic.

A double layer LB film on HOPG shows a contact angle value of 79º (Fig 14), value that is lower than the value of 90º obtained on bare HOPG, indicating a higher hydrophilicity in respect to graphite probably due to the presence of Zn and N atoms in the Pc. On the other hand, a LB film on mica shows a contact angle value of 55º (Fig 14), value that is higher than the value of 18º on bare mica, indicating a lower hydrophilicity in respect to mica, and confirming the presence of the PcZn film.

Table. Contact angles formed by water on different surfaces.

| Mica | HOPG | Mica-t.BuPcZn | HOPG-t-BuPcZn |
|---|---|---|---|
| 18º | 90º | 55º | 79º |

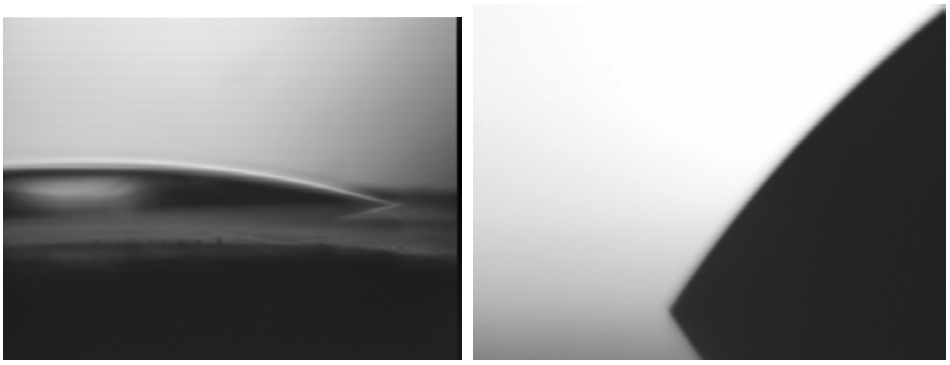

Water on mica water on t-buznpc(LB)/mica

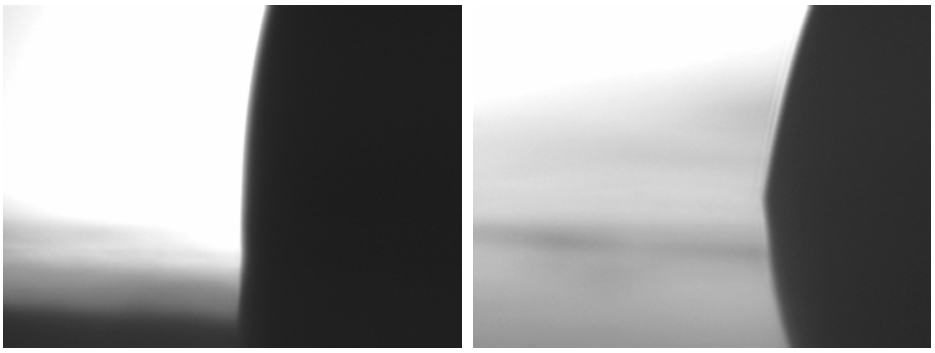

Water on HOPG water on t-buznpc(LB)/HOPG

Figure 14. Contact angle of water droplets on mica, on HOPG and on films of t-buznpc formed on theses substrates.

## 4. Medición de θ sobre materials RPG

**Objetivo**

Medir los ángulos de contacto de los 5 materiales Boston más utilizados: Boston ES, Boston EO, Boston EQ, Boston XO y Boston XO2.

Comprobar cómo se modifican las propiedades de humectabilidad de los materiales anteriores al sumergirlos durante una semana en soluciones acondicionadoras. Se utilizaron 3 tipos diferentes: Boston Simplus, Boston Acondiconador y Concare Solucion Acondicionadora.

**Método**

Se utilizaron 15 botones en bruto de materiales Boston ES, EO, EQ, XO y XO2. Se aclararon con agua destilada y se secaron con papel secante. La técnica utilizada para medir los ángulos de contacto fue mediante la gota sésil (gota-en-aire). Se utilizo una micropipeta para formar una gota de 2 microlitros de agua destilada pura. Mediante una cámara digital adaptada a un goniómetro se capturaron las imágenes de cada gota sobre cada material. Una vez obtenida las imágenes para los materiales en bruto y sin acondicionar, se sumergieron, cada uno de ellos, en solución humectante; 5 botones en Boston Simplus, 5 botones en Boston Acondiconador y 5 botones en Concare Solucion Acondicionadora.
Tras una semana en humectante se extrajeron los materiales y a continuación se tomaran dos capturas en diferente estado:
1. Recién extraído el material y secado con papel secante.
2. Aclarado con agua destilada y secado de nuevo con papel secante.

Posteriormente con el programa Adobe Photoshop se midieron los ángulos de contacto (Imagen 1 y 2).

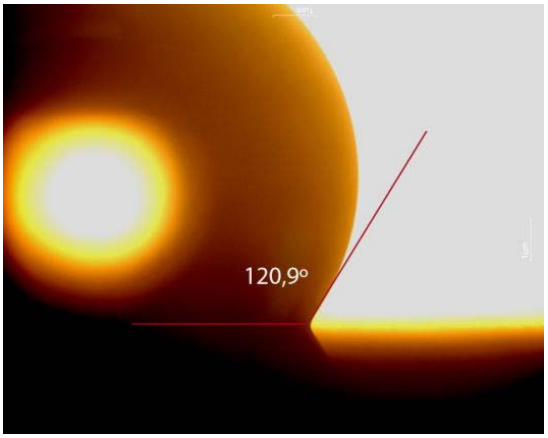


Imagen 1: Ángulo de Contacto en material Boston ES sin tratar

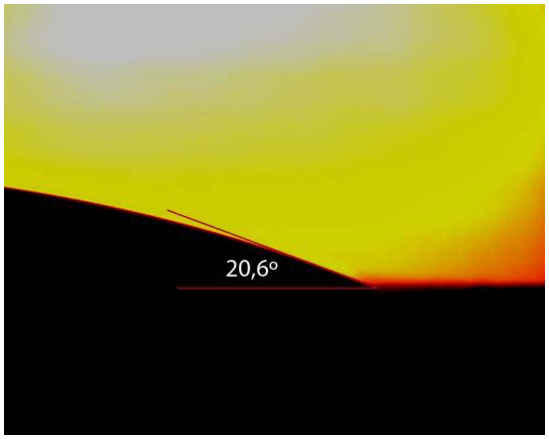


Imagen 2: Ángulo de contacto en material Boston ES humectado con Concare Solución Acondicionadora

**Resultados de las mediciones de los ángulos de contacto**

Los valores de los ángulos de contacto de los materiales sin tratar ni humectar son superiores a 90º por lo que se pueden considerar hidrófobos, tal como se muestra en la tabla 1. Sin embargo, al depositar los materiales en acondicionadores (humectantes) durante una semana, las propiedades de humectabilidad varían considerablemente, mostrando valores claramente por debajo de 90º, convirtiéndose en materiales marcadamente hidrofílicos. Una vez aclarado el material con agua y vuelto a secar con papel secante se observa un aumento del ángulo de contacto pero sin volver a los valores iniciales.

Tabla 0. Nombres comerciales, materiales y ángulo de retroceso de las lentes Boston usadas en el estudio (ver también Anexo).

| **Nombre comercial** | **Material** | **θ retroceso** |
|---|---|---|
| **Boston XO2** | **Hexafocon B** | **38º** |
| **Boston XO** | **Hexafocon A** | **49º** |
| **Boston EO** | **Enflufocon B** | **49º** |
| **Boston ES** | **Enflufocon A** | **52º** |
| **Boston EQ (Equalens)** | **Itafluorofocon A** | **30º** |

Tabla1. Medidas de los ángulos de contacto del material en seco, tal y como llega al laboratorio antes de tornearlo, pulirlo y limpiarlo.

| Material | Sin tratar |
|---|---|
| **ES** | 113,4±9.6 |
| **EO** | 115,6±11,7 |
| **EQ** | 116,8±7,4 |
| **XO** | 114,0±15,2 |
| **XO2** | 115,4±16,0 |

Tabla 2. Medidas de los ángulos de contacto de los materiales acondicionados en: B Simplus (Boston Simplus). S (secado). A/S (Aclarado y secado). B ACOND (Boston Acondicionador) S (secado). A/S (Aclarado y secado). CONCARE (Concare Solución Acondicionadora. S (secado). A/S (Aclarado y secado).

| **Material** | **B SIMPLUS S** | **B SIMPLUS A/S** | **B ACOND S** | **B ACOND A/S** | **CONCARE S** | **CONCARE A/S** |
|---|---|---|---|---|---|---|
| **ES** | 29,6±3,5 | 71,5±2,5 | 38,3±0,0 | 62,5±1,2 | 22,6±2,82 | 43,8±0,0 |
| **EO** | 39,4±0,3 | 61±0,8 | 31,9±1,1 | 75±0,0 | 27,1±3,0 | 38,3±0,0 |
| **EQ** | 44,7±6,3 | 51,5±0,9 | 37,25±0,9 | 76±0,0 | 33,9±0,0 | 66,4±0,0 |
| **XO** | 46,25±1,7 | 79,3±1,6 | 47,6±5,7 | 77,6±0,0 | 26,5±1,0 | 59±1,9 |
| **XO2** | 61,55±1,0 | 51,3±0,0 | 27,5±1,5 | 42,9±0,0 | 28,5±0,0 | 51,6±0,8 |

Tabla 3. Valor del ángulo contacto medio de los materiales sin tratar, humectados con Boston Simplus, Boston acondicionador y Concare Solución Acondicionadora. Únicamente secados (S). Aclarados y secados (A/S).

| | **Material sin tratar** | **B SIMPLUS S** | **B SIMPLUS A/S** | **B ACOND S** | **B ACOND A/S** | **CONCARE S** | **CONCARE A/S** |
|---|---|---|---|---|---|---|---|
| **Ángulo medio** | 115,0±1,3 | 44,3±11,6 | 62,9±12,4 | 36,5±7,6 | 66,8±14,6 | 27,7±4,1 | 51,8±11,3 |

## Conclusiones

Los materiales sin tratar son marcadamente hidrofóbicos, los tratamientos de humectabilidad proporcionados por los acondicionadores logran reducir estos valores hasta conseguir que estos materiales se conviertan en hidrofílicos. Una vez tratados los materiales con humectantes estos conservan su carácter hidrofílico incluso después de aclararse con agua. De los 3 acondicionadores, Boston simplus, Boston Acondicionador y Concare Solución Acondicionadora, existen diferencias de cómo se humectan los materiales en función del acondicionador seleccionado. Los mejores resultados se han obtenido con los humectados con Concare Solución Acondicionadora.

El bajo ángulo de contacto hallado en los materiales sin tratar hace suponer que existe una influencia positiva la tornear y pulir el material, tal y como se procedería en la fabricación de la lente de contacto. Po consiguiente, en estudio en más profundidad y con los materiales tratados igual que las lentes de contacto definitivas podría ser de ayuda para acercarnos más a la realidad de cuáles son los ángulos de humectabilidad reales en las lentes de contacto fabricadas en este tipo de materiales.

## 5.Ángulos de contacto de varias lágrimas artificiales

Les llàgrimes utilitzades en aquest estudi han estat*: Acuaiss Drops* multi dosis 6 mL, *Blink®contacts* multi dosis 10 mL, *Theratears®* mono dosis 0,6 mL i *Acuaiss Bany ocular.*
A continuació descriurem les composicions de cadascuna d'aquestes llàgrimes artificials emprades:

*Acuaiss Drops:*
Àcid hialuronic, hidroxietilcel·lulosa, clorur sòdic, tetraborat sòdic, àcid bòric, EDTA (àcid etilendiamintetraacètic) disòdic 0,02% i polihexanida 0,0001%.

*Blink® contacts:*
Hialuronat sòdic al 0,15%, OcuPure® conservant al 0,005%, clorur de calci (di hidratat), clorur potàssic, clorur sòdic, tampó de borat, clorur de magnesi i aigua destil·lada.

*Theratears®:*
Cada dosis unitària conté 0,6 ml de carboximetilcel·lulosa de sodi a al 0,25%, clorur de sodi, clorur de potassi, bicarbonat de sodi, clorur de calci, clorur de magnesi, fosfat de sodi, solució tampó de borat i aigua purificada.

Acuaiss Bany ocular:
Àcid hialurònic i polihexametilè biguanida al 0.0002%, clorur sòdic, fosfat disòdic, fosfat monosòdic en aigua purificada.

Hem fet totes les mesures en el laboratori mantenint en tot moment una temperatura constant de 22.5 ±0.5 ºC.

Material:
Microscopi horitzontal, càmera CCD, placa de PMMA, Micropipeta i llàgrimes artificials

Procediment:
Per mesurar l'angle de contacte hem dipositat diferents gotes en una placa de PMMA i mitjançant un microscopi horitzontal hem mesurat l'angle de contacte de les gotes de les diferents llàgrimes artificials.
Hem realitzat fotografies amb una càmera CCD i posteriorment hem mesurat l'angle amb un programa informàtic. Hem realitzat 6 mesures per llàgrima.

La taula indica els resultats del angle de contacte de cada llàgrima artificial mesurat mitjançant la tècnica del microscopi horitzontal. S'observa que les llàgrimes artificials presenten un valor d'angle de contacte molt similar entre si, i lleugerament inferior respecte a l'aigua.

**Taula. Angle de contacte**

| Angle de contacte/º | AIGUA | ACUAISS ® | BLINK ® | THER ATEA RS® | ACUAISS BAÑO® |
|---|---|---|---|---|---|
| Mesura 1 | 61,8 | 55,2 | 55,5 | 55 | 53,3 |
| Mesura 2 | 59 | 54,3 | 54,8 | 55,4 | 52 |
| Mesura 3 | 62,1 | 54,2 | 55,5 | 56,7 | 52,1 |
| Mesura 4 | 60,3 | 54,9 | 55,4 | 53,5 | 53,1 |
| Mesura 5 | 61,2 | 54 | 55,9 | 55,6 | 52 |
| Mesura 6 | 62 | 53 | 54,8 | 53,5 | 53 |
| *Mitjana* | *61,1* | *54,3* | *55,3* | *54,9* | *52,6* |
| *Desviació estàndard* | *1,2* | *0,7* | *0,4* | *1,3* | *0,6* |

Imatges

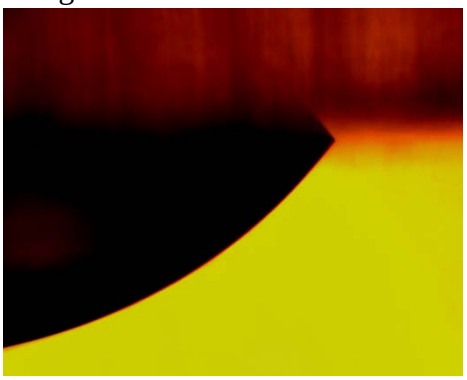

Acuaiss baño

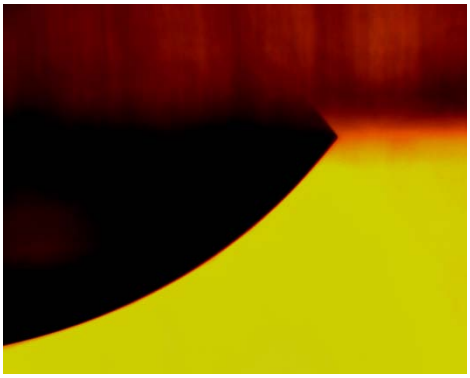

Acuaiss drops

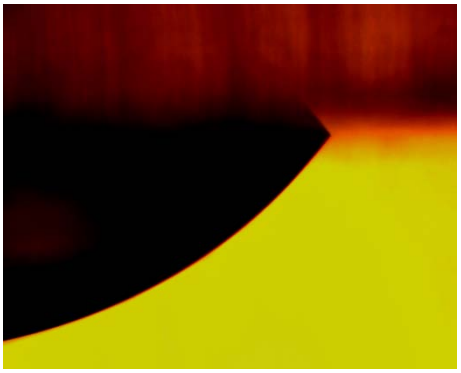

Blink contacts

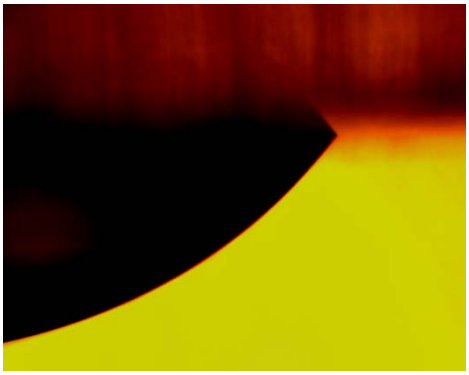

Theratears

# Annex: Figures, imatges d'angles de contacte.

## 1. Angle de contacte sobre diferents materials

S'ha mesurat l'angle de contacte de l'aigua sobre diferents superfícies de materials inorgànics, com mica, nitrur de silici, carboni vitri i grafit (HOPG). A les figures es mostren gotes d'aigua sobre aquestes superfícies, i en la taula es recullen els valors de l'angle de contacte.

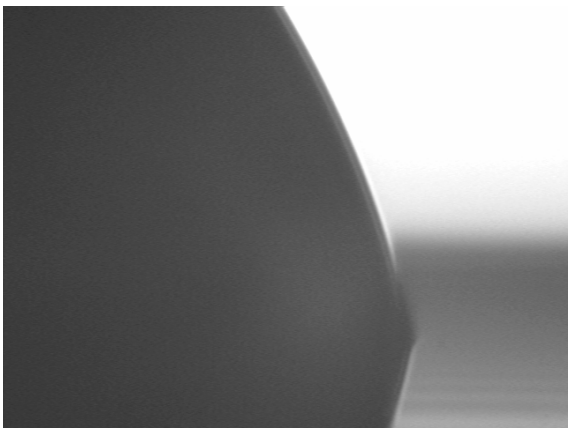

Cvitri aig5

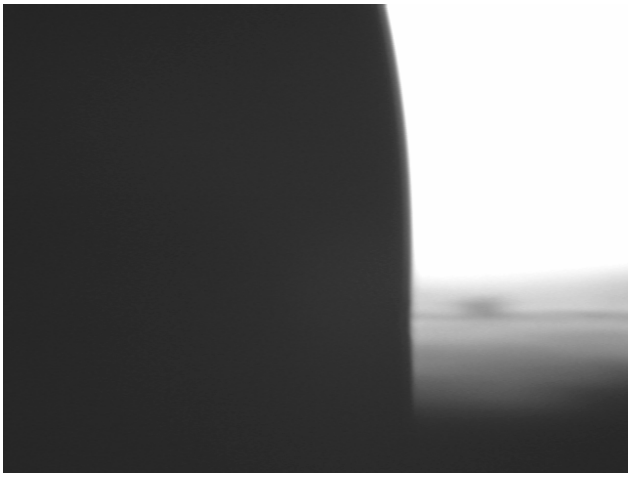

HOPG aig4

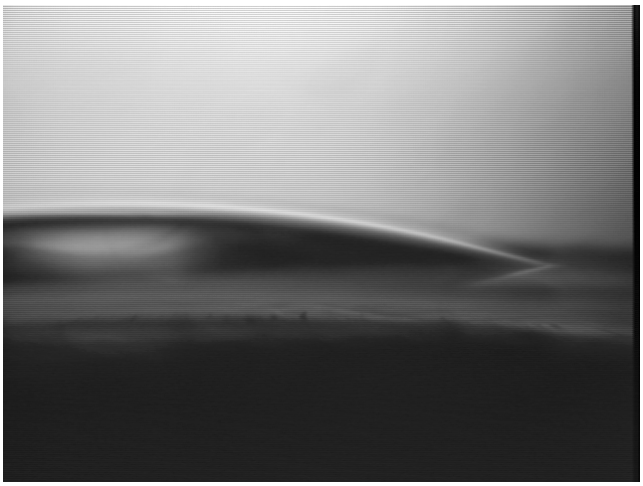

Mica 2

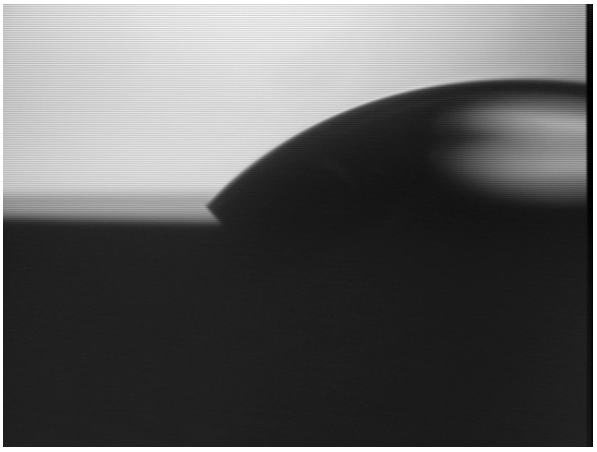

SiN7

Angles de contacte de l'aigua amb:

| mica | Nitrur silici | Carboni vitri | Grafit HOPG |
|---|---|---|---|
| 18º | 51º | 86º | 90º |

## 2. Angle de contacte sobre superficies modificades

Quan sobre la superficie d'un material es posa una pel·lícula d'un altre material o una pel·lícula molecular, l'angle de contacte es veu modificat. En les figures es mostren gotes formades sobre mica o HOPG recubertes de monocapes o multicapes de compostos macrocíclics, com ftalocianines o tiomacrocicle.

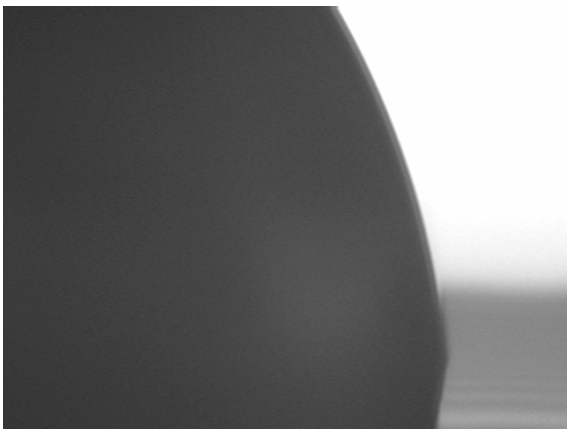

L13 aig2 θ=83º

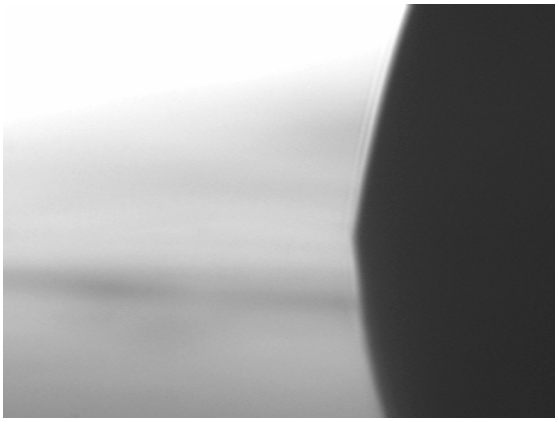

HOPG Pczn1

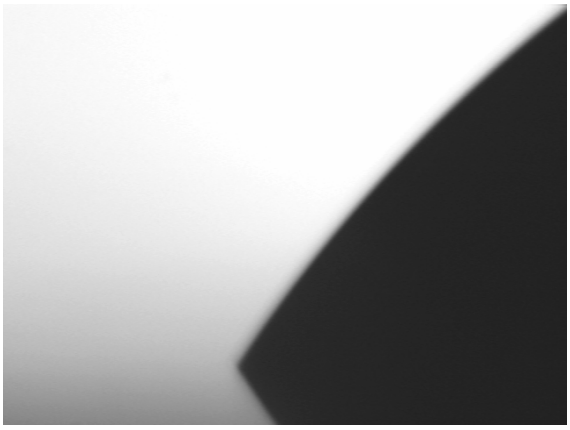

Mica pczn1

Angles de contacte de l'aigua sobre:

| | | | |
|---|---|---|---|
| Mica-t-BuPcZn | HOPG-t-BuPcZn | ¿-L13 | |
| 55º | 79º | 83º | |

## 3. Angle de contacte de materials RPG

Imágenes muestra de gotas de agua sobre materiales RPG. Los ángulos de contacto se midieron sobre varias gotas y varios tacos de material.

Materiales en seco

EO sec (EO 1-1 TT)

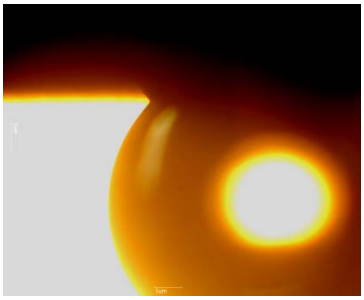

EQ sec (EQ 1-1 h2o)

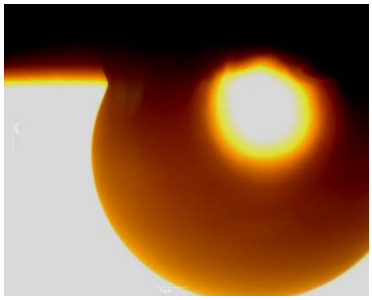

ES sec (ES 1-1 TT)

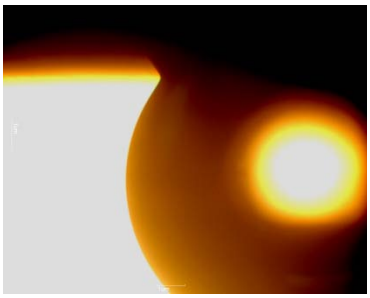

XO2 sec (XO2 1-1 TT)

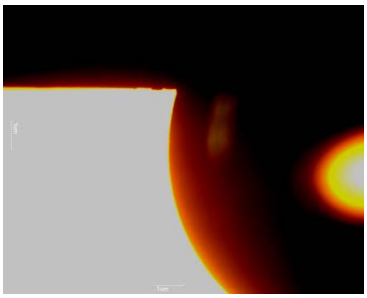

XO sec (XO 1-1 TT)

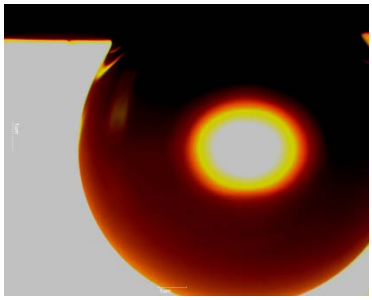

Materiales humectados.

Solución 1

secado

EO EQ ES


XO2 XO

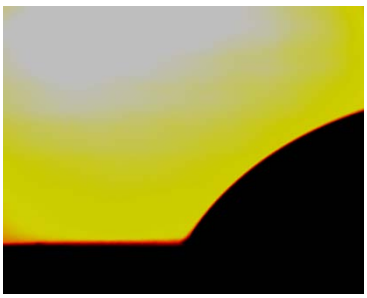


Aclarado y secado

EO EQ ES

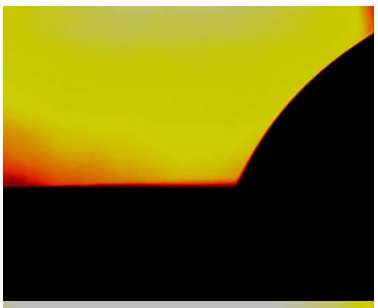
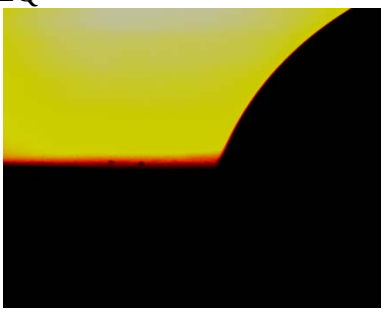


XO2 XO

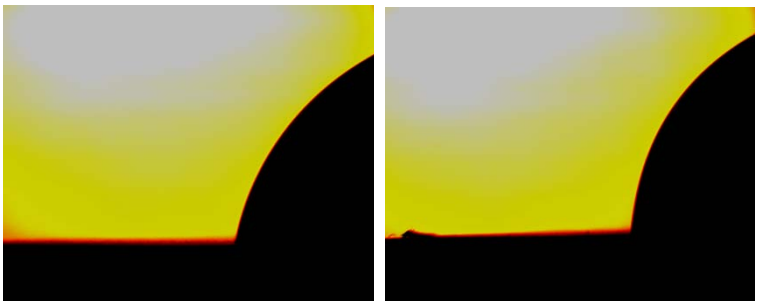

Solución 2

Secado

EO EQ ES

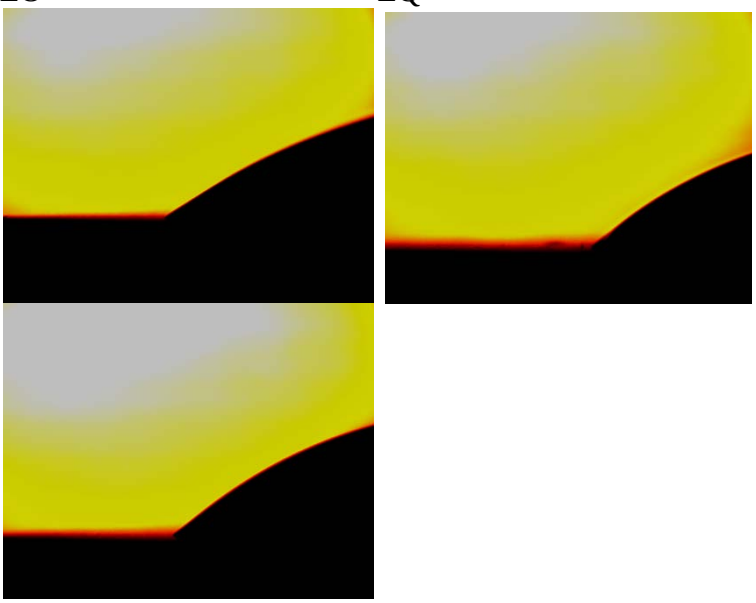

XO2 XO

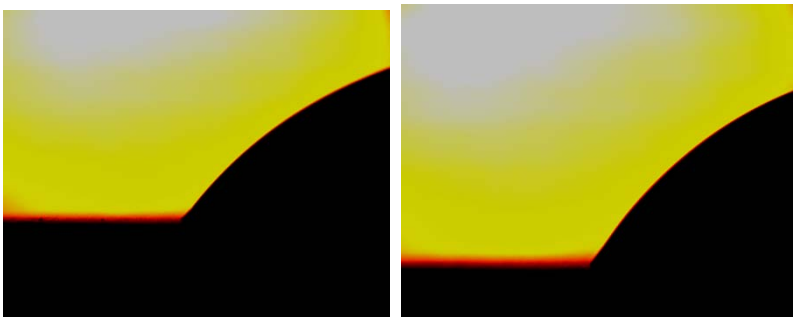

Aclarado y secado

EO EQ ES

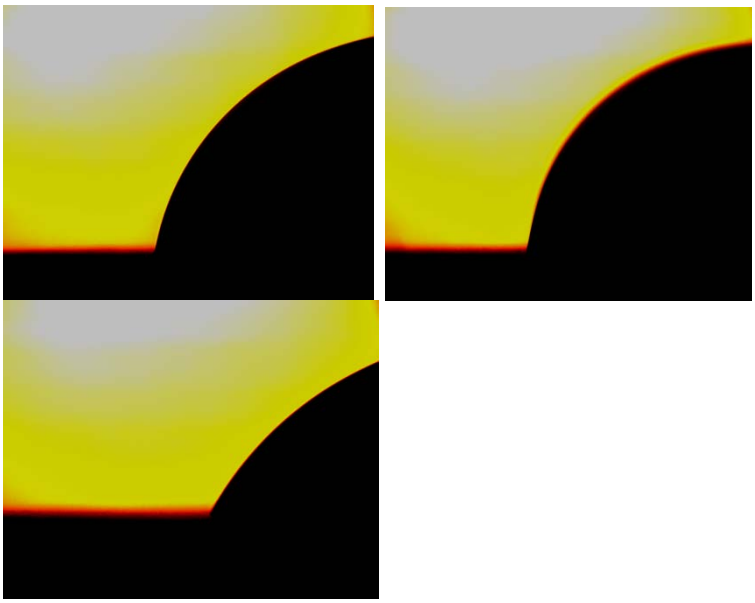

XO2 XO

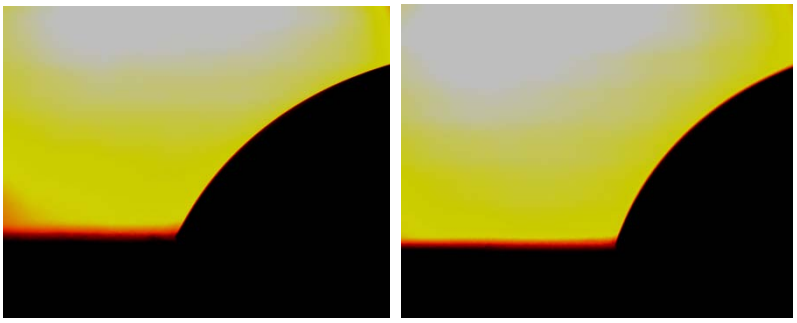

Solución 3

Secado

EO EQ ES

XO2 XO

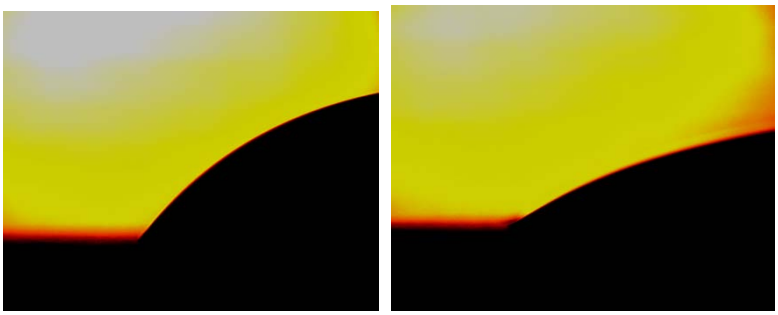

Aclarado y secado

EO

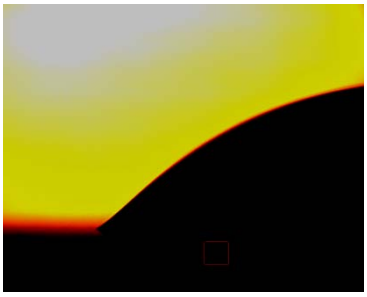

EQ

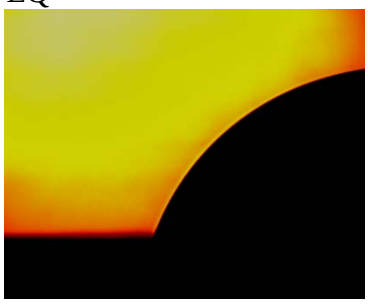

ES

XO2

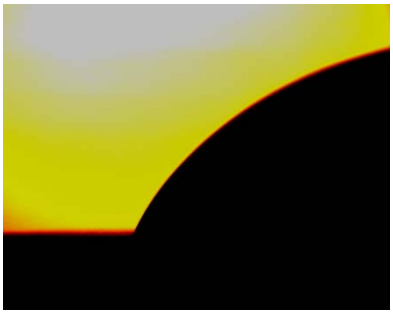

XO

# Annex: Lents Contacte

## Boston Equalens II

A high Dk gas permeable (GP) lens material formulated for daily or extended wear. Available in a wide range of parameters to suit most fitting situations.

### Indications/Features

- Myopia
- Hyperopia
- Astigmatism
- Daily wear
- Extended wear
- Overnight Orthokeratology

### Material Properties

| | |
|---|---|
| Trade Name: | Boston Equalens II |
| Material Name: | oprifocon A |
| Oxygen Permeability (Dk): | 85* |
| Wetting Angle: | (Captive Bubble) 30 deg. |
| Hardness: | (Rockwell R) 114 |
| Saline Absorption: | 1.0% |
| Refractive Index: | 1.423 |
| Specific Gravity: | 1.24 |
| Tint: | Blue |

*polarographic method (ISO/Fatt)

## Boston IV

A GP lens material suited for daily wear use. Available in a wide range of parameters to suit most fitting situations.

### Indications/Features

- Myopia
- Hyperopia
- Astigmatism
- Daily wear

### Material Properties

| | |
|---|---|
| Trade Name: | Boston IV |
| Material Name: | itafocon B |
| Oxygen Permeability (Dk): | 19* |
| Wetting Angle: | (Captive Bubble) 17 deg. |
| Hardness: | (Rockwell R) 117 |
| Saline Absorption: | 1.0% |
| Refractive Index: | 1.469 |
| Specific Gravity: | 1.10 |
| Tint: | Blue, Electric Blue, Clear |

*polarographic method (ISO/Fatt)

# Boston 7

Boston 7 contact lenses were designed as an improvement on earlier daily wear gas permeable lens. Boston 7 lenses are balanced lenses whose improved impact resistance and oxygen permeability make them an excellent choice for patient's interested in daily wear lenses. Boston 7 utilizes innovative technological innovations in basic polymer chemistry to achieve a lens that offers a balance between the effects of low and high dk materials.

## Polymer Technology (Bausch & Lomb)

- **Material...**satafocon A
- **DK...**49
- **Specific Gravity...**1.220
- **Base Curve...**Custom Fit
- **Diameter...**Custom Fit
- **Sphere Power...**Custom Fit
- **Wetting angle...**54
- **Color...**Blue, Ice Blue
- **Designs...**Aspheric, Bifocal, Toric, Bi-Toric, Front Toric, Back Toric

# BOSTON RXD

***Product Information:***

A strong, easily processed, RGP lens material for daily wear use. Available in a wide range of parameters to suit most fitting situations. The physical characteristics of the BOSTON® RXD polymer were designed to facilitate the fabrication of high quality lenses in a wide range of lens designs. Boston® RXD is available with UV absorbers.

- MATERIAL NAME: itafocon A

***Availability:*** These are made-to-order, 2-3 business days

- OXYGEN PERMEABILITY: (Dk) 24
- WETTING ANGLE: 39

# Boston XO2

Bausch + Lomb *Boston* products continue to *Lead The Way In GP Technology* with the introduction of our first hyper Dk gas permeable material – *Boston $XO_2$*. This premium GP material offers outstanding oxygen permeability (141 Dk using the ISO/Fatt method) without compromising wettability, stability or comfort.


This new GP material combines a Hyper Dk of 141* for excellent oxygen transmissibility with the stability, wettability and performance of a lower Dk material. *Boston $XO_2$* is inherently wettable, making plasma treatment optional. This material has received FDA clearance for daily wear for ametropia and certain irregular corneal conditions.

It is available in a variety of handling tints, with or without UV absorber.

* ISO/Fatt method

## Key Features and Benefits

- More oxygen for your patients' corneal health and overall comfort.
- Inherently wettable material, making plasma treatment optional.
- Provides the stability generally found in low to mid Dk GP materials.

## Additional Product Information

- Boston XO2 Patient Instructions (246.84 KB, PDF)
- Package Insert (276.31 KB, PDF)
- Package Insert Orthok (392.09 KB, PDF)

## Indications

- Daily wear
- Myopia
- Hyperopia
- Astigmatism

- Presbyopia

In addition it is cleared for irregular corneal conditions such as:

- Keratoconus
- Pellucid marginal degeneration
- Following penetrating keratoplasty
- Post lasik

## Material Properties

| | |
|---|---|
| Trade Name: | Boston $XO_2$ (hexafocon B) Rigid Gas Permeable Contact Lens |
| Material Name: | (hexafocon B) Rigid Gas Permeable Contact Lens |
| Oxygen Permeability – Edge Corrected** | 141* |
| Oxygen Permeability – Non-Edge Corrected** | 161* |
| Wetting Angle: | (Captive Bubble) 38 deg. |
| Hardness: | (Shore D) 78 (Rockwell) 101 |
| Saline Absorption: | 0.3% |
| Refractive Index: | 1.424 |
| Specific Gravity: | 1.19 |
| Tint: | Blue, Ice Blue, Violet, Green<br>Red, Yellow (daily wear orthokeratology) |

*ISO FATT Method: DK Units = x $10^{-11}$ (cm3 $O_2$)(cm)/[(sec)($cm^2$)(mmHg)] @ 35°C

## Plasma Treatment

Lenses manufactured from Boston $XO_2$ can be plasma treated in the same manner as other Boston materials. However, Boston $XO_2$ provides the stability of lower Dk materials and is inherently wettable, making plasma treatment optional.

Ask your Authorized Boston Manufacturer for more details.

## Boston XO


*Boston XO* is a tough, stable, high Dk material that can be made into a wide variety of special designs for demanding visual needs. Boston XO has an ISO/Fatt Dk of 100 with a proven record of international success as a premium extra oxygen exceptional stability GP material.

### Additional Product Information

- Package Insert (276.31 KB, PDF)

### Indications/Features

- Myopia
- Hyperopia
- Astigmatism
- Presbyopia
- Daily wear

### Material Properties

| | |
|---|---|
| Trade Name: | Boston XO |
| Material Name: | hexafocon A |
| Oxygen Permeability (Dk): | 100* |
| Wetting Angle: | (Captive Bubble) 49 deg. |
| Hardness: | (Rockwell R) 112 |
| Saline Absorption: | 1.0% |
| Refractive Index: | 1.415 |
| Specific Gravity: | 1.27 |
| Tint: | Blue, Ice Blue, Violet, Green |

*polarographic method (ISO/Fatt)

## Boston EO gas permeable lens material

*Boston* EO is the only GP material that combines a high-Dk of 58* with the proven performance of Boston ES and the patented *AERCOR* architecture.

## Indications/Features

- Myopia
- Hyperopia
- Astigmatism
- Presbyopia
- Daily wear

## Material Properties

| | |
|---|---|
| Trade Name: | *Boston* EO |
| Material Name: | enflufocon B |
| Oxygen Permeability (Dk): | 58* |
| Wetting Angle: | (Captive Bubble) 49 deg. |
| Hardness: | (Rockwell R) 114 |
| Saline Absorption: | 1.0% |
| Refractive Index: | 1.429 |
| Specific Gravity: | 1.23 |
| Tint: | Blue, Ice Blue, Green, Gray, Brown |

*polarographic method (ISO/Fatt)

## Boston ES

A GP lens material for daily wear that is formulated from the patented AERCOR architecture.

### Indications/Features

- Myopia
- Hyperopia
- Astigmatism
- Presbyopia
- Daily wear

### Material Properties

| | |
|---|---|
| Trade Name: | Boston ES |
| Material Name: | enflufocon A |
| Oxygen Permeability (Dk): | 18* |
| Wetting Angle: | (Captive Bubble) 52 deg. |
| Hardness: | (Rockwell R) 118 |
| Saline Absorption: | 1.0% |
| Refractive Index: | 1.443 |
| Specific Gravity: | 1.22 |
| Tint: | Blue, Ice Blue, Green, Gray, Brown |

*polarographic method (ISO/Fatt)

| NAME | MATERIAL / DK | WETTING ANGLE | COLORS | INDEX OF REFRACTION | SP GR |
|---|---|---|---|---|---|
| **POLYMER TECHNOLOGY CORP.**   | | | | | |
| Boston II | itafocon B<br>12 DK | 20.0 | blue | 1.471 | 1.13 |
| Boston IV | itafocon B<br>19 DK | 17.0 | blue | 1.469 | 1.10 |
| Boston EQ | itafluorofocon A<br>47 DK | 30.0 | blue | 1.439 | 1.19 |
| Boston EQ2 | oprifocon A<br>85 K | 30.0 | blue<br>red(Ortho-K), yello(Ortho-K) | 1.423 | 1.24 |
| Boston EO | enflufocon A<br>58 DK | 49.0 | blue, ice blue, green<br>gray, brown, electric blue | 1.429 | 1.23 |
| Boston ES | enflufocon A<br>18 DK | 52.0 | blue, ice blue, green<br>gray, brown, clear | 1.443 | 1.22 |
| Boston XO | hexafocon A<br>100 DK | 49.0 | blue, ice blue, green, violet<br>red(Ortho-K), yellow(Ortho-K) | 1.415 | 1.27 |

## Annex: Bibliografia recent sobre angle de contacte

Adhesion and friction properties of micro/nano-engineered superhydrophobic/hydrophobic surfaces
Y. Song, R. Premachandran Nair, M. Zou, Y.A. Wang
Thin Solid Films 518 (2010) 3801–3807

Hydrophobic micro/nano-engineered surfaces (MNESs) with good adhesion and frictional performances were fabricated by the combination of aluminum-induced crystallization (AIC) of amorphous silicon (a-Si) and octadecyltrichlorosilane (OTS) coating. The AIC of a-Si technique was used to produce silicon micro/nano-textured surfaces, while an OTS self-assembled monolayer was used to lower the surface energies of the textured surfaces. The wetting properties of the MNESs were studied using a video-based contact angle measurement system. The adhesion and friction properties of the MNESs were investigated using a TriboIndenter. This study shows that the adhesion and frictional performances of all MNESs are significantly improved compared to untreated silicon substrate surfaces, and the adhesion and frictional performances of the OTS-modified textured surfaces strongly correlate to their surface wetting property, i.e., the larger the water contact angle, the better the adhesion and frictional performances of the OTS-modified textured surfaces.

Contact angle hysteresis on fluoropolymer surfaces
H. Tavana, D. Jehnichen, K. Grundke, M.L. Hair, A.W. Neumann
Advances in Colloid and Interface Science 134–135 (2007) 236–248

Abstract
Contact angle hysteresis of liquids with different molecular and geometrical properties on high quality films of four fluoropolymers was studied. A number of different causes are identified for hysteresis. With n-alkanes as probe liquids, contact angle hysteresis is found to be strongly related to the configuration of polymer chains. The largest hysteresis is obtained with amorphous polymers whereas the smallest hysteresis occurs for polymers with ordered molecular chains. This is explained in terms of sorption of liquid by the solid and penetration of liquid into the polymer film. Correlation of contact angle hysteresis with the size of n-alkane molecules supports this conclusion.
On the films of two amorphous fluoropolymers with different molecular configurations, contact angle hysteresis of one and the same liquid with “bulky” molecules is shown to be quite different. On the surfaces of Teflon AF 1600,with stiff molecular chains, the receding angles of the probe liquids are independent of contact time between solid and liquid and similar hysteresis is obtained for all the liquids. Retention of liquid molecules on the solid surface is proposed as the most likely cause of hysteresis in these systems. On the other hand, with EGC-1700 films that consist of flexible chains, the receding angles are strongly time-dependent and the hysteresis is large. Contact angle hysteresis increases even further when liquids with strong dipolar intermolecular forces are used. In this case, major reorganization of EGC-1700 chains due to contact with the test liquids is suggested as the cause. The effect of rate of motion of the three-phase line on the advancing and receding contact angles, and therefore contact angle hysteresis, is investigated. For low viscous liquids, contact angles are independent of the drop front velocity up to ~10 mm/min. This agrees with the results of an earlier study that showed that the rate-dependence of the contact angles is an issue only for liquids with high viscosity.

Sliding behavior of liquid droplets on tilted Langmuir–Blodgett surfaces
Murielle Bouteau, Sophie Cantin, Fewzi Benhabib, Françoise Perrot
Journal of Colloid and Interface Science 317 (2008) 247–254

**Abstract**
The sliding behavior of liquid droplets on inclined Langmuir–Blodgett surfaces was investigated. The critical sliding angle defined as the tilt angle of the surface at which the drop slides down as well as the

advancing and receding contact angles was measured for five different liquids on five surfaces. In addition, the contact line geometry was analyzed at critical sliding angle. The experimental relationship between the surface tension forces resulting from contact angle hysteresis and the weight of the drop was compared to theoretical predictions. Even though the shape of the drop bases was found as skewed ellipses, a model assuming parallel-sided elongated drops is shown to describe reasonably the experimental values. This result probably indicates the main influence of the capillary forces at the rear and front edges of the drop with respect to that exerted on the lateral sides.

Normal capillary forces
Hans-Jürgen Butt, Michael Kappl
Advances in Colloid and Interface Science 146 (2009) 48–60

A liquid meniscus between two lyophilic solid surfaces causes an attractive force, the capillary force. The meniscus can form by capillary condensation or by accumulation of adsorbed liquid. Under ambient conditions and between hydrophilic surfaces, capillary forces usually dominate over other surface forces.
They are relevant in many processes occurring in nature and technical applications, for example the flow of granular materials and friction between surfaces. Here we review normal capillary forces, focusing on a quantitative description with continuum theory. After introducing the capillary force between spherical surfaces, we extend the discussion to other regular and irregular surfaces. The influence of surface roughness is considered. In addition to capillary forces at equilibrium, we also describe the process of meniscus formation. Assumptions, limits, and perspectives for future work are discussed.

Facile electrochemical route to directly fabricate hierarchical spherical cupreous microstructures: Toward superhydrophobic surface
Liang Wang, Shaojun Guo, Shaojun Dong
Electrochemistry Communications DOI: 10.1016/j.elecom.2008.01.034

A templateless, surfactantless, electrochemical route is proposed to directly fabricate hierarchical spherical cupreous microstructures (HSCMs) on an indium tin oxide (ITO) substrate. The as-prepared HSCMs have been characterized by scanning electron microscopy (SEM), energy-dispersive X-ray (EDX) analysis, X-ray photoelectron spectroscopy (XPS) and X-ray diffraction (XRD). The HSCMs prepared by simple potentiostatic technique exhibit hierarchical spherical microstructures with higher roughness. After further chemisorption of a self-assembled monolayer of *n*dodecanethiol, the as-prepared compact surface becomes superhydrophobic with a contact angle as high as 152°.

Hysteresis during contact angles measurement
M. Elena Diaz, Javier Fuentes, Ramon L. Cerro c, Michael D. Savage
Journal of Colloid and Interface Science 343 (2010) 574–583

A theory, based on the presence of an adsorbed film in the vicinity of the triple contact line, provides a molecular interpretation of intrinsic hysteresis during the measurement of static contact angles. Static contact angles are measured by placing a sessile drop on top of a flat solid surface. If the solid surface has not been previously in contact with a vapor phase saturated with the molecules of the liquid phase, the solid surface is free of adsorbed liquid molecules. In the absence of an adsorbed film, molecular forces configure an advancing contact angle larger than the static contact angle. After some time, due to an evaporation/adsorption process, the interface of the drop coexists with an adsorbed film of liquid molecules as part of the equilibrium configuration, denoted as the static contact angle. This equilibrium configuration is metastable because the droplet has a larger vapor pressure than the surrounding flat film. As the drop evaporates, the vapor/liquid interface contracts and the apparent contact line moves towards the center of the drop. During this process, the film left behind is thicker than the adsorbed film and molecular attraction results in a receding contact angle, smaller than the equilibrium contact angle.

Review of non-reactive and reactive wetting of liquids on surfaces

Girish Kumar, K. Narayan Prabhu
Advances in Colloid and Interface Science 133 (2007) 61–89

Wettability is a tendency for a liquid to spread on a solid substrate and is generally measured in terms of the angle (contact angle) between the tangent drawn at the triple point between the three phases (solid, liquid and vapour) and the substrate surface. A liquid spreading on a substrate with no reaction/absorption of the liquid by substrate material is known as non-reactive or inert wetting whereas the wetting process influenced by reaction between the spreading liquid and substrate material is known as reactive wetting. Young's equation gives the equilibrium contact angle in terms of interfacial tensions existing at the three-phase interface. The derivation of Young's equation is made under the assumptions of spreading of non-reactive liquid on an ideal (physically and chemically inert, smooth, homogeneous and rigid) solid, a condition that is rarely met in practical situations. Nevertheless Young's equation is the most fundamental starting point for understanding of the complex field of wetting. Reliable and reproducible measurements of contact angle from the experiments are important in order to analyze the wetting behaviour. Various methods have been developed over the years to evaluate wettability of a solid by a liquid. Among these, sessile drop and wetting balance techniques are versatile, popular and provide reliable data. Wetting is affected by large number of factors including liquid properties, substrate properties and system conditions. The effect of these factors on wettability is discussed. Thermodynamic treatment of wetting in inert systems is simple and based on free energy minimization where as that in reactive systems is quite complex. Surface energetics has to be considered while determining the driving force for spreading. Similar is the case of spreading kinetics. Inert systems follow definite flow pattern and in most cases a single function is sufficient to describe the whole kinetics. Theoretical models successfully describe the spreading in inert systems. However, it is difficult to determine the exact mechanism that controls the kinetics since reactive wetting is affected by a number of factors like interfacial reactions, diffusion of constituents, dissolution of the substrate, etc. The quantification of the effect of these interrelated factors on wettability would be useful to build a predictive model of wetting kinetics for reactive systems.

Importance of pinning effect of wetting in super water-repellent surfaces
Kazutomo Kurogi, Hu Yanc, Kaoru Tsujii
Colloids and Surfaces A: Physicochem. Eng. Aspects 317 (2008) 592–597

We have first found that the pinning effect of wetting plays an important role as the 4th mechanism for the super water-repellent surfaces in some cases, particularly in the surfaces consisting of pillar structures. In such cases the plot of cos ϑR (ϑR: contact angle of a liquid on a rough surface) versus cos ϑ (ϑ: that on the flat surface) deviates remarkably from the expected curves of the Wenzel and the Cassie/Baxter theories, and one can judge the dominance of pinning effect in the super water-repellency from this plot. In addition the super water-repellent surfaces resulting from the pinning effect is not in the thermodynamically equilibrium state, but in the metastable one when the contact angle on the flat surface is smaller than 90◦.

A simple approach to fabricate regenerable superhydrophobic coatings
Jin Yang, Zhaozhu Zhang, Xuehu Men, Xianghui Xu, Xiaotao Zhu
Colloids and Surfaces A: Physicochem. Eng. Aspects 367 (2010) 60–64

A simple approach is proposed to fabricate a regenerable superhydrophobic coating constructed by spraying metal alkylcarboxylate dispersion on any substrates. This dispersion is prepared by the reaction of metal salt and alkylcarboxyl acid in ethanol solution. The sprayed coating with the flowerlike hierarchical structures shows stable super-repellent behavior for several oily liquids such as ethylene glycol and benzyl alcohol. The advantage of the present approach is that the superhydrophobic performance can be easily repaired by spraying the dispersion again when the coating surfaces are damaged, and the cheap coating materials and simple fabrication approach allow the local repair at anytime and almost anywhere.

A Strategy of Fast Reversible Wettability Changes of WO3 Surfaces between

Superhydrophilicity and Superhydrophobicity
Changdong Gu, Jun Zhang, Jiangping Tu
Journal of Colloid and Interface Science DOI: 10.1016/j.jcis.2010.08.064

As-prepared WO3 nanostructure films on alumina or tungsten substrates by a facile hydrothermal method exhibit a superhydrophilic property. An effective strategy is proposed to control the wettability of WO3 films in a reversible manner between superhydrophilicity and superhydrophobicity with a rapid response. By controlling the process of adsorption/desorption of *n*-dodecanethiol associated with the light-induced plating Ag nano-grains on WO3 nanostructures, it only takes about 25 min to fulfill the wettability change from superhydrophilicity to superhydrophobicity, and only 30 s to finish the reversed change. Moreover, the contact angles of WO3 surface can be tuned by controlling the etching time of superhydrophobic WO3 surfaces in a solution of nitric acid containing 5 mM sodium dodecyl benzene sulfonate. Electrowetting process is successfully demonstrated to trap a water drop onto the superhydrophobic WO3 surfaces. Considering WO3 is one of typical electrochromic materials, researches on the effect of coupling between electrowetting and electrochromic properties would be more promising.

Layer-by-layer fabrication of broad-band superhydrophobic antireflection coatings in near-infrared region
Lianbin Zhang, Yang Li, Junqi Sun, Jiacong Shen
Journal of Colloid and Interface Science 319 (2008) 302–308

Broad-band superhydrophobic antireflective (AR) coatings in near infrared (NIR) region were readily fabricated on silicon or quartz substrates by a layer-by-layer (LbL) assembly technique. First, a porous poly(diallyldimethylammonium chloride) (PDDA)/SiO2 nanoparticle multilayer coating with AR property was prepared by LbL deposition of PDDA and 200 nm SiO2 nanoparticles. PDDA was then alternately assembled with sodium silicate on the PDDA/SiO2 nanoparticle coating to prepare a two-level hierarchical surface. Superhydrophobic AR coating with a water contact angle of 154◦ was finally obtained after chemical vapor deposition of a layer of fluoroalkylsilane on the hierarchical surface. Quartz substrate with the as-fabricated superhydrophobic AR coating has a maximal transmittance above 98% of incidence light in the NIR region, which is increased by five percent compared with bare quartz substrate. Simultaneously, the superhydrophobic property endows the AR coating with water-repellent ability. Such superhydrophobic AR coatings can effectively avoid the disturbance of water vapor on their AR property and are expected to be applicable under humid environments.

Reversible Conversion of Water-Droplet Mobility from Rollable to Pinned on a Superhydrophobic Functionalized Carbon Nanotube Film
Jin Yang, Zhaozhu Zhang, Xuehu Men, Xianghui Xu, Xiaotao Zhu
Journal of Colloid and Interface Science DOI: 10.1016/j.jcis.2010.02.040

Poly(acrylic acid)-block-polystyrene (PAA-b-PS) functionalized multiwall carbon nanotubes (MWNTs) were prepared by nitroxide-mediated “living” free-radical polymerization. The product functionalized MWNTs (MWNT-PAA-b-PS) contained 20% by weight PAA-b-PS based on the infrared spectroscopy analysis and thermal gravimetric analysis. Such MWNT-PAA-b-PS nanoparticles can be used in spray coating method to fabricate superhydrophobic MWNT films, and water droplet mobility on the superhydrophobic film can be reversibly converted from rollable to pinned through adjusting the appearance of PAA chains on the topmost surface of the film. Switching mechanism has been discussed in detail. We also directly observed the air-solid-liquid interface from the above of a water droplet by a microscope to confirm the superhydrophobic states, and proved that the transition between the wettability states appeared on the same surface with reversible conversion of water droplet mobility

Wettability Switching Techniques on Superhydrophobic Surfaces
Nicolas Verplanck, Yannick Coffinier, Vincent Thomy, Rabah Boukherroub

Nanoscale Res Lett (2007) 2:577–596 DOI 10.1007/s11671-007-9102-4

Abstract The wetting properties of superhydrophobic surfaces have generated worldwide research interest. A water drop on these surfaces forms a nearly perfect spherical pearl. Superhydrophobic materials hold considerable promise for potential applications ranging from self cleaning surfaces, completely water impermeable textiles to low cost energy displacement of liquids in lab-on-chip devices. However, the dynamic modification of the liquid droplets behavior and in particular of their wetting properties on these surfaces is still a challenging issue. In this review, after a brief overview on superhydrophobic states definition, the techniques leading to the modification of wettability behavior on superhydrophobic surfaces under specific conditions: optical, magnetic, mechanical, chemical, thermal are discussed. Finally, a focus on electrowetting is made from historical phenomenon pointed out some decades ago on classical planar hydrophobic surfaces to recent breakthrough obtained on superhydrophobic surfaces.

Wetting of low-energy surfaces
N.V. Churaev, V.D. Sobolev
Advances in Colloid and Interface Science 134–135 (2007) 15–23

Abstract
Results of current theoretical methods for the calculation of contact angles on low-energy surfaces as functions of composition of solution and surface properties are reviewed.

Title: Facile approach for preparation of stable water-repellent nanoparticle coating
Authors: Xia Zhang, Yonggang Guo, Zhijun Zhang, Pingyu Zhang
*Applied Surface Science* DOI: doi:10.1016/j.apsusc.2012.04.119

The present study reports a very simple and low-cost dip-coating method for the preparation of fluorine-free water-repellent SiO2 nanoparticle coating. The coating has a high water contact angle of 169° and a sliding angle of 7°, showing superhydrophobic property. The coating demonstrates good adhesion on substrates and the long-term stability. Importantly, the coating also demonstrates superhydrophobicity in the wide pH range of corrosive liquids. It is found that a piece of glass coated with superhydrophobic coatings can not only float freely on water surface but also exhibit striking loading capacities.

Superhydrophobic surfaces: From natural to biomimetic to functional
Zhiguang Guo, Weimin Liu, Bao-Lian Su
Journal of Colloid and Interface Science 353 (2011) 335–355

Nature is the creation of aesthetic functional systems, in which many natural materials have vagarious structures. Inspired from nature, such as lotus leaf, butterfly' wings, showing excellent superhydrophobicity, scientists have recently fabricated a lot of biomimetic superhydrophobic surfaces by virtue of various smart and easy routes. Whilst, many examples, such as lotus effect, clearly tell us that biomimicry is dissimilar to a simple copying or duplicating of biological structures. In this feature article, we review the recent studies in both natural superhydrophobic surfaces and biomimetic superhydrophobic surfaces, and highlight some of the recent advances in the last four years, including the various smart routes to construct rough surfaces, and a lot of chemical modifications which lead to superhydrophobicity. We also review their functions and applications to date. Finally, the promising routes from biomimetic superhydrophobic surfaces in the next are proposed.

Superhydrophilic and superhydrophobic nanostructured surfaces via plasma treatment
Juan P. Fernández-Blázquez, Daniela Fell, Elmar Bonaccurso, Aránzazu del Campo

Journal of Colloid and Interface Science 357 (2011) 234–238

Polyethylene terephthalate (PET) films have been structured with isolated nanofibrils and fibril bundles using oxidative plasma treatments with increasing etching ratios. The transition from fibrils to bundles was smooth and it was associated with a significant reduction in the overall top area fraction and with the development of a second organisation level at a larger length scale. This increased complexity was reflected in the surface properties. The surfaces with two-level substructures showed superhydrophilic and superhydrophobic properties depending on the surface chemistry. These properties were preserved during prolonged storage and resisted moderate mechanical stress. By combining different contact angle and drop impact measurements, the optimum surface design and plasma processing parameters for maximizing stability of the superhydrophobic or superhydrophilic properties of the PET films were identified.

Fabrication and characterization of hierarchical nanostructured smart adhesion surfaces
Hyungoo Lee, Bharat Bhushan
Journal of Colloid and Interface Science 372 (2012) 231–238

The mechanics of fibrillar adhesive surfaces of biological systems such as a Lotus leaf and a gecko are widely studied due to their unique surface properties. The Lotus leaf is a model for superhydrophobic surfaces, self-cleaning properties, and low adhesion. Gecko feet have high adhesion due to the high micro/ nanofibrillar hierarchical structures. A nanostructured surface may exhibit low adhesion or high adhesion depending upon fibrillar density, and it presents the possibility of realizing eco-friendly surface structures with desirable adhesion. The current research, for the first time uses a patterning technique to fabricate smart adhesion surfaces: single- and two-level hierarchical synthetic adhesive structure surfaces with various fibrillar densities and diameters that allows the observation of either the Lotus or gecko adhesion effects. Contact angles of the fabricated structured samples were measured to characterize their wettability, and contamination experiments were performed to study for self-cleaning ability. A conventional and a glass ball attached to an atomic force microscope (AFM) tip were used to obtain the adhesive forces via force-distance curves to study scale effect. A further increase of the adhesive forces on the samples was achieved by applying an adhesive to the surfaces.

Title: Mechanism study of condensed drops jumping on super-hydrophobic surfaces
Authors: T.Q. Liu, W. Sun, X.Y. Sun, H.R. Ai
*Colloids and Surfaces A: Physicochem. Eng. Aspects* DOI: doi:10.1016/j.colsurfa.2012.08.063

**Abstract**
The out-of-plane jumping motion of coalesced condensed drops on super-hydrophobic surfaces can potentially enhance dropwise condensation greatly. But the jumping mechanism is not clear. In this paper, the initial shape of a coalesced droplet is determined based on the conservation of drop interface free energy (IFE) and viscous dissipation energy before and after two or more condensed droplets merge. The coalesced drop is in unstable state with a driving force to reduce its base radius toward equilibrium state. Then, the driving force and resistance on three-phase contact line (TPCL) are analyzed during the drop transformation. And the dynamic equation describing the shape conversion of the droplet is proposed and solved. The jumping height of a merged drop is determined according to the up moving speed of drop gravity center when the base radius of the droplet reduces to 0. The calculation results show that a coalesced droplet on flat surface can transform its shape limitedly. It can not jump since its transformation stops before it comes to its equilibrium state. A wetted drop on rough surfaces is even more difficult to transform and jump because of the greater TPCL resistance. However, on a two-tier surface, a partially wetted drop impaling only the micro-scale roughness exhibits a shape transition to Cassie state and possible jumping upon coalescence if the micro and nanostructure parameters are suitable. Furthermore, after the coalescence of two or more Cassie state drops with their scale range from tens micrometer to millimeter on a textured surface, the merged composite drop can easily transform until its base radius becomes 0 and then jumps. A too small or too large merged drop will not jump because the

obvious viscous dissipation energy or drop gravity respectively dominates the behavior of the drop. Meanwhile the coalescence-induced jumping of two drops will also not take place if their scales are significantly different. It can be concluded that the key factors resulting in condensed drops jumping are the merged drop in unstable state with enough surplus IFE and small TPCL resistance on nano or micro-nano two-tier surfaces.

Evaporation of pure liquid sessile and spherical suspended drops: A review
H. Yildirim Erbil
Advances in Colloid and Interface Science 170 (2012) 67–86

A sessile drop is an isolated drop which has been deposited on a solid substrate where the wetted area is limited by a contact line and characterized by contact angle, contact radius and drop height. Diffusioncontrolled evaporation of a sessile drop in an ambient gas is an important topic of interest because it plays a crucial role in many scientific applications such as controlling the deposition of particles on solid surfaces, in ink-jet printing, spraying of pesticides, micro/nano material fabrication, thin film coatings, biochemical assays, drop wise cooling, deposition of DNA/RNA micro-arrays, and manufacture of novel optical and electronic materials in the last decades. This paper presents a review of the published articles for a period of approximately 120 years related to the evaporation of both sessile drops and nearly spherical droplets suspended from thin fibers. After presenting a brief history of the subject, we discuss the basic theory comprising evaporation of micrometer and millimeter sized spherical drops, self cooling on the drop surface and evaporation rate of sessile drops on solids. The effects of drop cooling, resultant lateral evaporative flux and Marangoni flows on evaporation rate are also discussed. This review also has some special topics such as drop evaporation on superhydrophobic surfaces, determination of the receding contact angle from drop evaporation, substrate thermal conductivity effect on drop evaporation and the rate evaporation of water in liquid marbles.

Effect of pattern size and geometry on the use of Cassie–Baxter equation for superhydrophobic surfaces
C. Elif Cansoy, H. Yildirim Erbil, Orhan Akar, Tayfun Akin
Colloids and Surfaces A: Physicochem. Eng. Aspects 386 (2011) 116– 124

Cassie–Baxter equation depending on the extent of liquid/solid interfacial contact area was generally used in the past to estimate water contact angles on superhydrophobic surfaces. However, there are objections refuting the contact area based equations and suggesting that the three-phase contact line determines the apparent contact angle. In this study, we tested the validity of Cassie–Baxter equation on superhydrophobic surfaces. 36 pattern samples made of square and 24 of cylindrical pillars were prepared by applying the DRIE technique on Si-wafers. Pillar side lengths and diameters were varied between 8 and 100 _m and the height of pillars was kept nearly constant between 30 and 34 _m. 18 square and 12 cylindrical patterns were coated by hydrophobic dimethyldichlorosilane vapor to obtain superhydrophobic surfaces.
Recent method of Erbil and Cansoy was used to test the validity of Cassie–Baxter equation to estimate the water contact angles on these superhydrophobic surfaces. It was found that Cassie–Baxter equation was valid only for some special pattern geometry. The factors affecting the applicability of the Cassie–Baxter equation such as geometric type of the pillars, size of pillars and separation distance between the pillars are discussed throughout the text.

The Cassie equation: How it is meant to be used
A.J.B. Milne, A. Amirfazli
Advances in Colloid and Interface Science 170 (2012) 48–55

A review of literature shows that the majority of papers cite a potentially incorrect form of the Cassie and Cassie–Baxter equations to interpret or predict contact angle data. We show that for surfaces wet with a composite interface, the commonly used form of the Cassie–Baxter equation, $\cos\theta c = f1 \cos\theta - (1-f)$, is only correct for the case of flat topped pillar geometry without any penetration of the liquid. In general, the original form of the Cassie–Baxter equation, $\cos\theta c = f1 \cos\theta 1 - f2$, with $f1+f2 \geq 1$, should be

used. The differences between the two equations are discussed and the errors involved in using the incorrect equation are estimated to be between ~3° and 13° for superhydrophobic surfaces. The discrepancies between the two equations are also discussed for the case of a liquid undergoing partial, but increasing, levels of penetration.
Finally, a general equation is presented for the transition/stability criterion between the Cassie–Baxter and Wenzel modes of wetting.

Evaporation of droplets on strongly and weakly pinning surfaces and dynamics of the triple line
Edward Bormashenko, Albina Musin, Michael Zinigrad
Colloids and Surfaces A: Physicochem. Eng. Aspects 385 (2011) 235– 240

Evaporation of water droplets deposited on metal and polymer substrates was studied. The evaporated droplet demonstrates different behavior on weakly pinning (polymer) and strongly pinning (metallic) surfaces. When deposited on polymer surfaces, the evaporated droplet is featured by stick-slip sliding, whereas on strong-pinning metallic surfaces it does not show such kind of motion and demonstrates the giant contact-angle hysteresis. Stick-slip motion of droplets is described satisfactorily by the Shanahan–Sefiane model relating this kind of motion to surmounting potential barriers caused by the pinning of the triple (three-phase) line. The experimentally established “stick” times coincide with the values predicted by the Shanahan–Sefiane theory. The values of potential barriers are reported. The notion of the equilibrium contact angle is refined.

A modified Cassie–Baxter relationship to explain contact angle hysteresis and anisotropy on non-wetting textured surfaces
Wonjae Choi, Anish Tuteja, Joseph M. Mabry, Robert E. Cohen, Gareth H. McKinley
Journal of Colloid and Interface Science 339 (2009) 208–216

The Cassie–Baxter model is widely used to predict the apparent contact angles obtained on composite (solid–liquid–air) superhydrophobic interfaces. However, the validity of this model has been repeatedly challenged by various research groups because of its inherent inability to predict contact angle hysteresis.
In our recent work, we have developed robust omniphobic surfaces which repel a wide range of liquids. An interesting corollary of constructing such surfaces is that it becomes possible to directly image the solid–liquid–air triple-phase contact line on a composite interface, using an electron microscope with non-volatile organic liquids or curable polymers. Here, we fabricate a range of model superoleophobic surfaces with controlled surface topography in order to correlate the details of the local texture with the experimentally observed apparent contact angles. Based on these experiments, in conjunction with numerical simulations, we modify the classical Cassie–Baxter relation to include a local differential texture parameter which enables us to quantitatively predict the apparent advancing and receding contact angles, as well as contact angle hysteresis. This quantitative prediction also allows us to provide an a priori estimation of roll-off angles for a given textured substrate. Using this understanding we design model substrates that display extremely small or extremely large roll-off angles, as well as surfaces that demonstrate direction-dependent wettability, through a systematic control of surface topography and connectivity.

**Annex: Aspectes teòrics (ref Wikipedia)**

## *High-energy vs. low-energy surfaces*

There are two main types of solid surfaces with which liquids can interact. Traditionally, solid surfaces have been divided into high-energy solids and low-energy types. The relative energy of a solid has to do with the bulk nature of the solid itself. Solids such as metals, glasses, and ceramics are known as 'hard solids' because the chemical bonds that hold them together (e.g., covalent, ionic, or metallic) are very strong. Thus, it takes a large input of energy to break these solids so they are termed “high energy.” Most molecular liquids achieve complete wetting with high-energy surfaces.

The other type of solids is weak molecular crystals (e.g., fluorocarbons, hydrocarbons, etc.) where the molecules are held together essentially by physical forces (e.g., van der Waals and hydrogen bonds). Since these solids are held together by weak forces it would take a very low input of energy to break them, and thus, they are termed “low energy.” Depending on the type of liquid chosen, low-energy surfaces can permit either complete or partial wetting.

### Wetting of low-energy surfaces

Low-energy surfaces primarily interact with liquids through dispersion (van der Waals) forces. William Zisman had several key findings in the work that he did:

- Zisman observed that cos θ increases linearly as the surface tension ($\gamma_{LV}$) of the liquid decreased. Thus, he was able to establish a rectilinear relation between cos θ and the surface tension ($\gamma_{LV}$) for various organic liquids.

A surface is more wettable when $\gamma_{LV}$ is low and when θ is low. He termed the intercept of these lines when the cos θ = 1, as the critical surface tension ($\gamma_c$) of that surface. This critical surface tension is an important parameter because it is a characteristic of only the solid.

Knowing the critical surface tension of a solid, it is possible to predict the wettability of the surface.

- The wettability of a surface is determined by the outermost chemical groups of the solid.
- Differences in wettability between surfaces that are similar in structure are due to differences in packing of the atoms. For instance, if a surface has branched chains, it will have poorer packing than a surface with straight chains.

## *Ideal solid surfaces*

An ideal solid surface is one that is flat, rigid, perfectly smooth, chemically homogeneous, and has zero contact angle hysteresis. Zero hysteresis implies that the advancing and receding contact angles are equal. In other words, there is only one thermodynamically stable contact angle. When a drop of liquid is placed on such a surface, the characteristic contact angle is formed as depicted in Fig. 1. Furthermore, on an ideal surface the drop will return to its original shape if it is disturbed. The following derivations apply only to ideal solid surfaces. In other words, they are only valid for the state in which the interfaces are not moving and the phase boundary line exists in equilibrium.


Figure 1: Droplet of water on an ideal surface.

## Minimization of energy, three phases

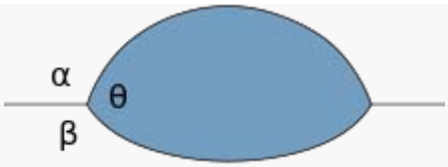


Figure 3: Coexistence of 3 fluid phases in mutual contact. α, β, and θ represent both the labels of the phases and the contact angles.

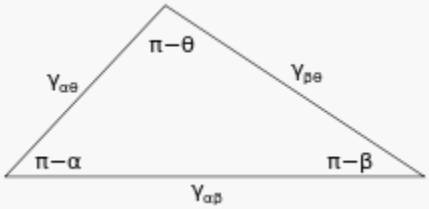


Figure 4: Neumann's triangle relating the surface energies and contact angles of 3 fluid phases coexisting in static equilibrium, as depicted in Figure 3.

Figure 3 shows the line of contact where three phases meet. In equilibrium, the net force per unit length acting along the boundary line between the three phases must be zero. The components of net force in the direction along each of the interfaces are given by:

$$\begin{aligned}
\gamma_{\alpha\theta} + \gamma_{\theta\beta}\cos\theta + \gamma_{\alpha\beta}\cos\alpha &= 0 \\
\gamma_{\alpha\theta}\cos\theta + \gamma_{\theta\beta} + \gamma_{\alpha\beta}\cos\beta &= 0 \\
\gamma_{\alpha\theta}\cos\alpha + \gamma_{\theta\beta}\cos\beta + \gamma_{\alpha\beta} &= 0
\end{aligned}$$

where α, β, and θ are the angles shown and $\gamma_{ij}$ is the surface energy between the two indicated phases. These relations can also be expressed by an analog to a triangle known as Neumann's triangle, shown in Figure 4. Neumann's triangle is consistent with the geometrical restriction that $\alpha + \beta + \theta = 2\pi$, and applying the law of sines and law of cosines to it produce relations that describe how the interfacial angles depend on the ratios of surface energies.

Because these three surface energies form the sides of a triangle, they are constrained by the triangle inequalities, $\gamma_{ij} < \gamma_{jk} + \gamma_{ik}$ meaning that no one of the surface tensions can exceed the sum of the other two. If three fluids with surface energies that do not follow these inequalities are brought into contact, no equilibrium configuration consistent with Figure 3 will exist.

### *Simplification to planar geometry, Young's relation*

If the β phase is replaced by a flat rigid surface, as shown in Figure 5, then β = π, and the second net force equation simplifies to theYoung equation,

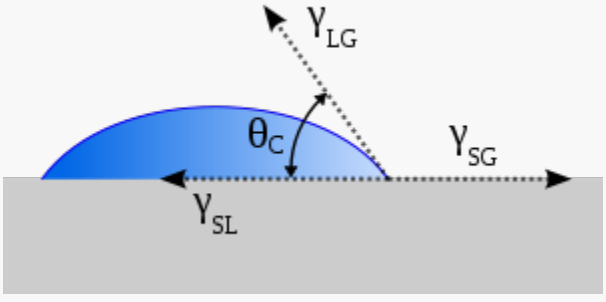


Figure 5: Contact angle of a liquid droplet wetted to a rigid solid surface.

$$\gamma_{SG} = \gamma_{SL} + \gamma_{LG}\cos\theta$$

which relates the surface tensions between the three phases: solid, liquid and gas. Subsequently this predicts the contact angle of a liquid droplet on a solid surface from knowledge of the three surface energies involved. This equation also applies if the "gas" phase is another liquid, immiscible with the droplet of the first "liquid" phase.

***Real smooth surfaces and the Young contact angle***

The Young equation assumes a perfectly flat and rigid surface. In many cases surfaces are far from this ideal situation, and two are considered here: the case of rough surfaces (see Non-ideal rough solid surfaces) and the case of smooth surfaces that are still real (finitely rigid). Even in a perfectly smooth surface a drop will assume a wide spectrum of contact angles ranging from the so-called **advancing contact angle**, $\theta_{\mathrm{A}}$, to the so-called **receding contact angle**, $\theta_{\mathrm{R}}$. The equilibrium contact angle ($\theta_{\mathrm{c}}$) can be calculated from $\theta_{\mathrm{A}}$ and $\theta_{\mathrm{R}}$ as was shown by Tadmor as,

$$\theta_{\mathrm{c}} = \arccos\left(\frac{r_{\mathrm{A}}\cos\theta_{\mathrm{A}} + r_{\mathrm{R}}\cos\theta_{\mathrm{R}}}{r_{\mathrm{A}} + r_{\mathrm{R}}}\right)$$

where

$$r_{\mathrm{A}} = \left(\frac{\sin^3\theta_{\mathrm{A}}}{2 - 3\cos\theta_{\mathrm{A}} + \cos^3\theta_{\mathrm{A}}}\right)^{1/3} \quad ; \quad r_{\mathrm{R}} = \left(\frac{\sin^3\theta_{\mathrm{R}}}{2 - 3\cos\theta_{\mathrm{R}} + \cos^3\theta_{\mathrm{R}}}\right)^{1/3}$$

***The Young–Dupré equation and spreading coefficient***

The Young–Dupré equation (Thomas Young 1805, Lewis Dupré 1855) dictates that neither $\gamma_{SG}$ nor $\gamma_{SL}$ can be larger than the sum of the other two surface energies. The consequence of this restriction is the prediction of complete wetting when $\gamma_{SG} > \gamma_{SL} + \gamma_{LG}$ and zero wetting when $\gamma_{SL} > \gamma_{SG} + \gamma_{LG}$. The lack of a solution to the Young–Dupré equation is an indicator that there is no equilibrium configuration with a contact angle between 0 and 180° for those situations.

A useful parameter for gauging wetting is the *spreading parameter S*,

$$S = \gamma_{SG} - (\gamma_{SL} + \gamma_{LG})$$

When $S > 0$, the liquid wets the surface completely (complete wetting). When $S < 0$, there is partial wetting.

Combining the spreading parameter definition with the Young relation yields the Young–Dupré equation:

$$S = \gamma_{LG}(\cos\theta - 1)$$

which only has physical solutions for θ when $S < 0$.

## *Non-ideal rough solid surfaces*

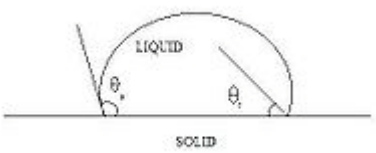

Figure 6: Schematic of advancing and receding contact angles.

Unlike ideal surfaces, real surfaces do not have perfect smoothness, rigidity, or chemical homogeneity. Such deviations from ideality result in phenomena called contact-angle hysteresis. Contact-angle hysteresis is defined as the difference between the advancing ($\theta_a$) and receding ($\theta_r$) contact angles

$$\mathrm{H} = \theta_a - \theta_r$$

In simpler terms, contact angle hysteresis is essentially the displacement of a contact line such as the one in figure 3, by either expansion or retraction of the droplet. Figure 6 depicts the advancing and receding contact angles. The advancing contact angle is the maximum stable angle, whereas the receding contact angle is the minimum stable angle. Contact-angle hysteresis occurs because there are many different thermodynamically stable contact angles on a non-ideal solid. These varying thermodynamically stable contact angles are known as metastable states.

Such motion of a phase boundary, involving advancing and receding contact angles, is known as dynamic wetting. When a contact line advances, covering more of the surface with liquid, the contact angle is increased and generally is related to the velocity of the contact line. If the velocity of a contact line is increased without bound, the contact angle increases, and as it approaches 180° the gas phase will become entrained in a thin layer between the liquid and solid. This is a kinetic non-equilibrium effect which results from the contact line moving at such a high speed that complete wetting cannot occur.

A well-known departure from ideality is when the surface of interest has a rough texture. The rough texture of a surface can fall into one of two categories: homogeneous or heterogeneous. A homogeneous wetting regime is where the liquid fills in the roughness grooves of a surface. On the other hand, a heterogeneous wetting regime is where the surface is a composite of two types of patches. An important example of such a composite surface is one composed of patches of both air and solid. Such surfaces have varied effects on the contact angles of wetting liquids. Cassie–Baxter and Wenzel are the two main models that attempt describe the wetting of textured surfaces. However, these equations only apply when the drop size is sufficiently large compared with the surface roughness scale.

## Wenzel's model

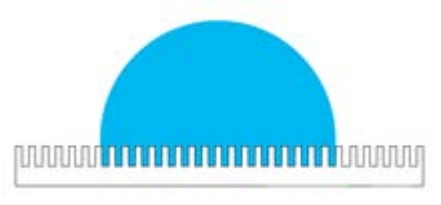

Figure 7: Wenzel model

The Wenzel model (Robert N. Wenzel 1936) describes the homogeneous wetting regime, as seen in Figure 7, and is defined by the following equation for the contact angle on a rough surface:

$$\cos\,\theta^* = r\cos\,\theta$$

where $\theta^*$ is the apparent contact angle which corresponds to the stable equilibrium state (i.e. minimum free energy state for the system). The roughness ratio, r, is a measure of how surface roughness affects a homogeneous surface. The roughness ratio is defined as the ratio of true area of the solid surface to the apparent area.

θ is the Young contact angle as defined for an ideal surface. Although Wenzel's equation demonstrates that the contact angle of a rough surface is different from the intrinsic contact angle, it does not describe contact angle hysteresis.

## Cassie–Baxter model

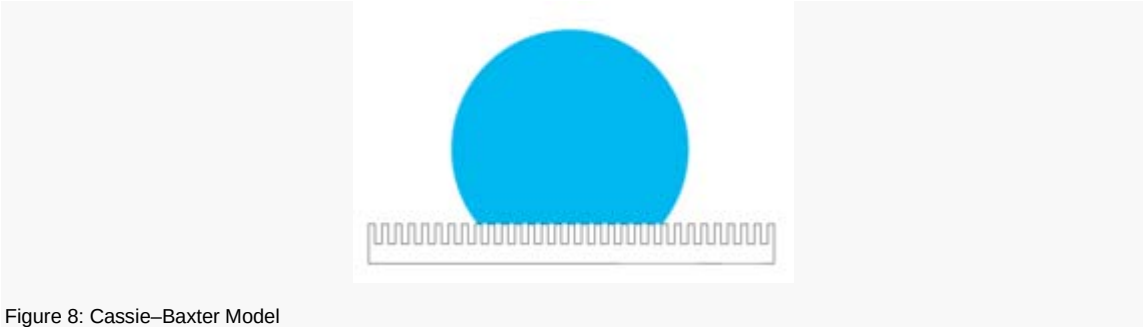

Figure 8: Cassie–Baxter Model

When dealing with a heterogeneous surface, the Wenzel model is not sufficient. A more complex model is needed to measure how the apparent contact angle changes when various materials are involved. This heterogeneous surface, like that seen in Figure 8, is explained using the Cassie–Baxter equation (Cassie's law):

$$\cos\,\theta^* = r_f\, f\, cos\,\theta_{\mathrm{Y}} + f\, - 1$$

Here the $r_f$ is the roughness ratio of the wet surface area and f is the fraction of solid surface area wet by the liquid. It is important to realize that when $f = 1$ and $r_f = r$, the Cassie–Baxter equations becomes the Wenzel equation. On the other hand, when there are many different fractions of surface roughness, each fraction of the total surface area is denoted by $f_i$.

A summation of all $f_i$ equals 1 or the total surface. Cassie–Baxter can also be recast in the following equation:

$$\gamma\cos\,\theta^* = \sum_{n=1}^{N} f_i(\gamma_{\mathrm{i,sv}} - \gamma_{\mathrm{i,sl}})$$

Here γ is the Cassie–Baxter surface tension between liquid and vapor, the $\gamma_{i,sv}$ is the solid vapor surface tension of every component and $\gamma_{i,sl}$ is the solid liquid surface tension of every component. A case that is worth mentioning is when the liquid drop is placed on the substrate and creates small air pockets underneath it. This case for a two-component system is denoted by:

$$\gamma\cos\,\theta^* = f_1(\gamma_{1,\mathrm{sv}} - \gamma_{1,\mathrm{sl}}) + (1 - f_1)\gamma$$

Here the key difference to notice is that the there is no surface tension between the solid and the vapor for the second surface tension component. This is because of the assumption that the surface of air that is exposed is under the droplet and is the only other substrate in the system. Subsequently the equation is then expressed as (1 – *f*). Therefore the Cassie equation can be easily derived from the Cassie–Baxter equation. Experimental results regarding the surface properties of Wenzel versus Cassie–Baxter systems showed the effect of pinning for a Young angle of 180° to 90°, a region classified under the Cassie–Baxter model. This liquid air composite system is largely hydrophobic. After that point a sharp transition to the Wenzel regime was found where the drop wets the surface but no further than edges of the drop.

## Cassie–Baxter to Wenzel transition

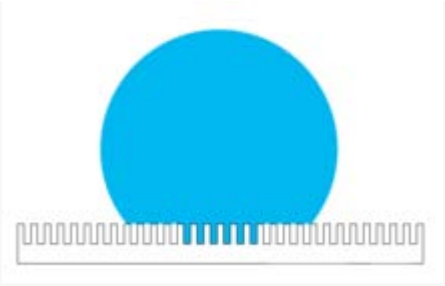

Figure 10: Mushroom state

In the Cassie–Baxter model, the drop sits on top of the textured surface with trapped air underneath. During the wetting transition from the Cassie state to the Wenzel state, the air pockets are no longer thermodynamically stable and liquid begins to nucleate from the middle of the drop, creating a "mushroom state," as seen in Figure 10. The penetration condition is given by the following equation:

$$\cos\,\theta_{\mathrm{C}} = \frac{\phi - 1}{r - \phi}$$

where

- $\theta_C$ is the critical contact angle
- $\Phi$ is the fraction of solid/liquid interface where drop is in contact with surface
- $r$ is solid roughness (for flat surface, r = 1)

Figure 11: Penetration front spreads beyond drop

The penetration front propagates to minimize the surface energy until it reaches the edges of the drop, thus arriving at the Wenzel state. Since the solid can be considered an absorptive material due to its surface roughness, this phenomenon of spreading and imbibition is called hemi-wicking. The contact angles at which spreading/imbibition occurs are between $0 \leq \theta < \pi/2$.

The Wenzel model is valid between $\theta_C < \theta < \pi/2$. If the contact angle is less than $\Theta_C$, the penetration front spreads beyond the drop and a liquid film forms over the surface. Figure 11 depicts the transition from the Wenzel state to the surface film state. The film smoothes the surface roughness and the Wenzel model no longer applies. In this state, the equilibrium condition and Young's relation yields:

$$\cos\,\theta^* = \phi\cos\,\theta_C + (1 - \phi)$$

By fine-tuning the surface roughness, it is possible achieves a transition between both super hydrophobic and super hydrophilic regions. Generally, the rougher the surface, the more hydrophobic it is.